

# Report

for the

**Marshall Plan Scholarship supported research stay**

at the group of Prof. Zhigang Suo

Allen E. and Marilyn M. Puckett Professor of Mechanics and Materials

[School of Engineering and Applied Sciences](#)

Harvard University

Cambridge, Massachusetts 02138

from 10/29/2012 to 02/28/2013

**Rainer Kaltseis**

PhD Student

at the

Department for Soft Matter Physics

Johannes Kepler University

<b>I. <u>EFFECT OF IMPEDANCE ON THE PERFORMANCE OF SOFT GENERATORS</u></b>	<b>3</b>
<b>I.1. INTRODUCTION</b>	<b>3</b>
<b>I.2. THEORY</b>	<b>6</b>
<b>I.3. CONCLUSION</b>	<b>12</b>
<b>I.4. OUTLOOK AND ACKNOWLEDGEMENT</b>	<b>13</b>
<b>II. <u>NATURAL RUBBER BASED SOFT GENERATORS ENABLING SUSTAINABLE AND LOW-COST ENERGY HARVESTING</u></b>	<b>14</b>
<b>II.1. INTRODUCTION</b>	<b>14</b>
<b>II.2. WAVE ENERGY CONVERTERS</b>	<b>15</b>
<b>II.3. ESTIMATING LCOE</b>	<b>20</b>
<b>II.4. ESTIMATING GREENHOUSE GAS EMISSIONS</b>	<b>24</b>
<b>II.5. POTENTIAL AND PRODUCTION OF GENERATION OF ELECTRICITY</b>	<b>24</b>
<b>II.6. MATERIAL PROPERTIES</b>	<b>26</b>
<b>II.7. DETERMINATION OF FRACTURE ENERGY</b>	<b>34</b>
<b>II.8. HYSTERESIS LOSS FOR ELASTOMERS</b>	<b>38</b>
<b>II.9. ENERGY CONVERSION</b>	<b>41</b>
<b>II.10. MODELLING OF BALLOON DEFORMATION</b>	<b>44</b>
<b>II.11. EXPERIMENTAL RESULTS</b>	<b>47</b>
<b>II.12. CONCLUSION</b>	<b>52</b>
<b>II.13. REFERENCES</b>	<b>53</b>

# **I. Effect of Impedance on the performance of soft generators**

## **I.1. Introduction**

Dielectric elastomer actuators and generators use membranes made of VHB, PDMS or even natural rubber as both a dielectric and actuation material at the same time[1–3]. A cornucopia of applications has been realized[4–7] some of them, such as loudspeakers[7] reaching into the high-frequency range for actuation. This poses a new challenge for the electrodes used in elastomer actuators and generators since the frequency at which their performance is acceptable is limited by their inertia and the electrical cut-off frequency of the capacitor – voltage source system  $\omega$ . The typical setup of a elastomer actuator/generator contains an elastomer membrane coated with compliant electrodes (see Figure I.1).

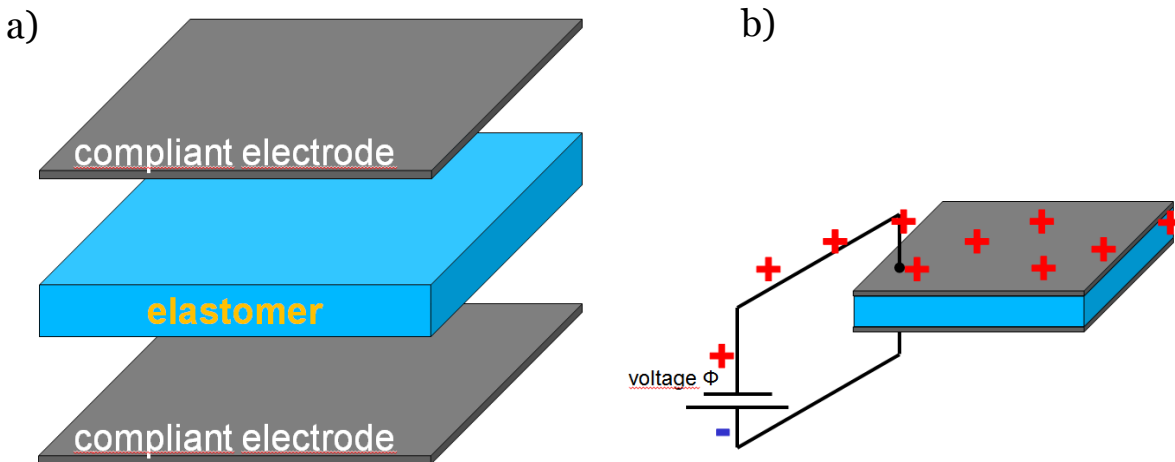


*Figure I.1. Typical setup of a dielectric elastomer actuator/generator. a) A piece of elastomer is sandwiched by two compliant electrodes to form a variable capacitor. b) This electrodes are then connected to an electrical circuit to perform either actuation of generation.*

In this setup the mechanical deformation is coupled to the state of the variable capacitor realized by the membrane. The speed of actuation is thus limited by the time needed to fully charge the membrane[8]. A commonly used material for compliant electrodes is carbon grease which has very good conductivity in a non-stretched state. Preliminary experiments have shown that upon application of large strains the resistivity of carbon grease electrodes increases exponentially. Further the resistivity increases when the electrodes dry up and the carbon particles accumulate into lumps which are not connected to the rest of the electrode.

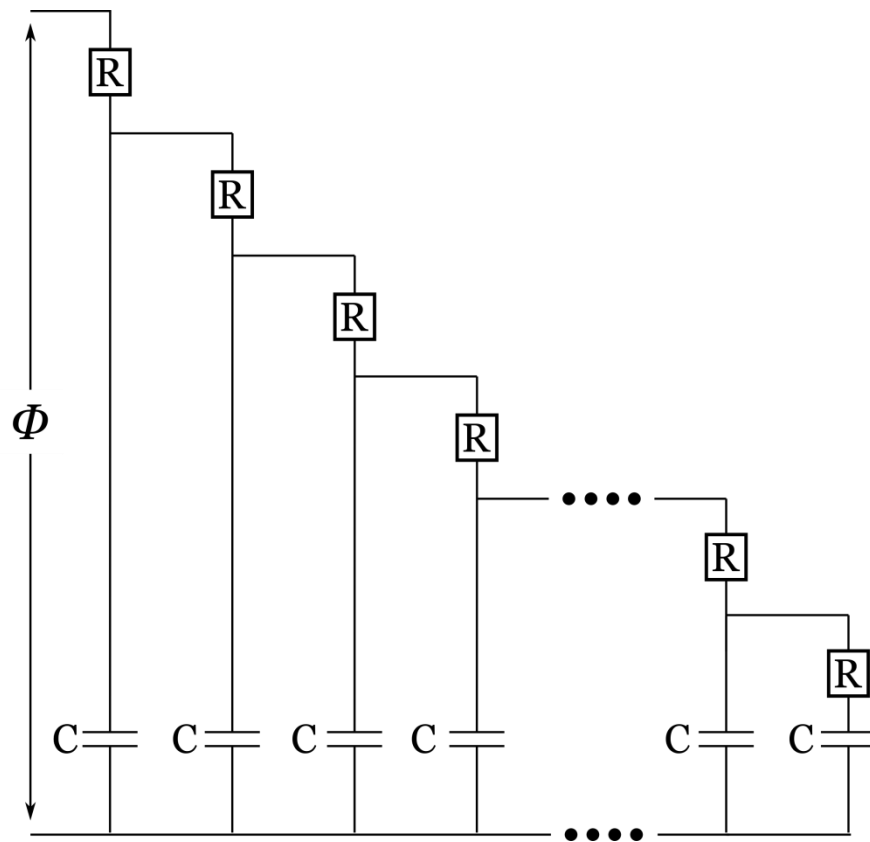
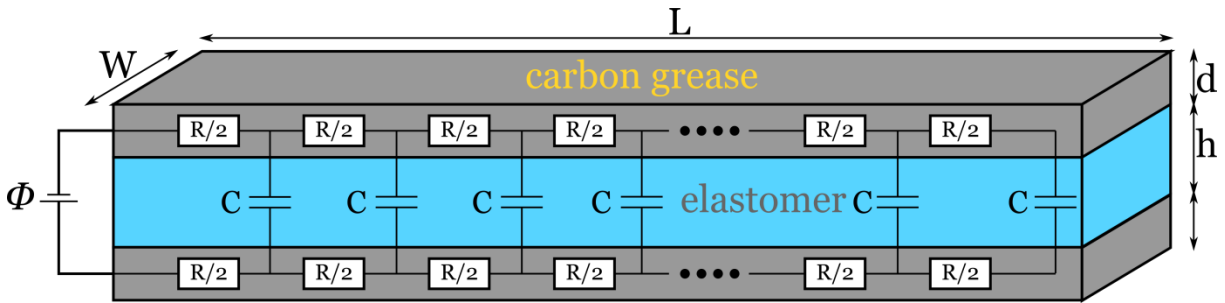


Figure I.2. **Circuit to describe a dielectric elastomer coated with bad electrodes.** a) Intuitive view of the setup. b) Equivalent circuit used for modeling the actuator/generator.

## I.2. Theory

Our approach to understand the effect of compliant electrodes with bad conductivity on the performance of elastomer actuators is to model the electrodes as discrete network of infinitesimal resistors and capacitors which are connected to build up an elongated strip of elastomer membrane. A sketch of this setup is given in Figure I.2. The resistance of the upper electrode  $R_0$  can be measured independently and is distributed to  $N$  individual serial resistors with resistance  $R$  such that

$$R = \frac{2R_0}{N} \quad (\text{I.1})$$

The capacitance of the dielectric elastomer is depicted geometrically by  $C_0 = \epsilon_0 \epsilon W L h^{-1}$  and distributed to  $N$  parallel capacitors with capacitance

$$C = \frac{C_0}{N} \quad (\text{I.2})$$

An approximate solution for the total impedance  $Z_t$  is found by realizing that for large number  $N$  the impedance does not change if on building block is added to the whole network. This can be formulated as

$$Z_t = R + \frac{1}{j\omega C + \frac{1}{Z_t}} \quad (I.3)$$

This approach results in a quadratic equation

$$Z_t^2 - R Z_t - \frac{R}{j\omega C} = 0 \quad (I.4)$$

with the solution

$$Z_t = \frac{R_0}{N} \pm \sqrt{\left(\frac{R_0}{N}\right)^2 + \frac{2R_0}{j\omega C_0}} \quad (I.5)$$

As the number of elements grows to infinity ( $N \rightarrow \infty$ ) only one term in (I.5) survives and the approximate total impedance is

$$Z_t \approx R_0 \sqrt{\frac{2}{j\omega R_0 C_0}} \quad (I.6)$$

The corresponding Bode-Plot of this system is shown in Figure I.3 and reveals no cut-off frequency and a constant phase angle of  $-45^\circ$ .

A more rigorous approach to calculating the total impedance is achieved by a bottom-up approach. We first look at one building block whose impedance is

$$Z_1 = R + \frac{1}{j\omega C} \quad (I.7)$$

Adding another building block in parallel we get

$$Z_2 = R + \frac{1}{j\omega C + 1/Z_1} \quad (I.8)$$

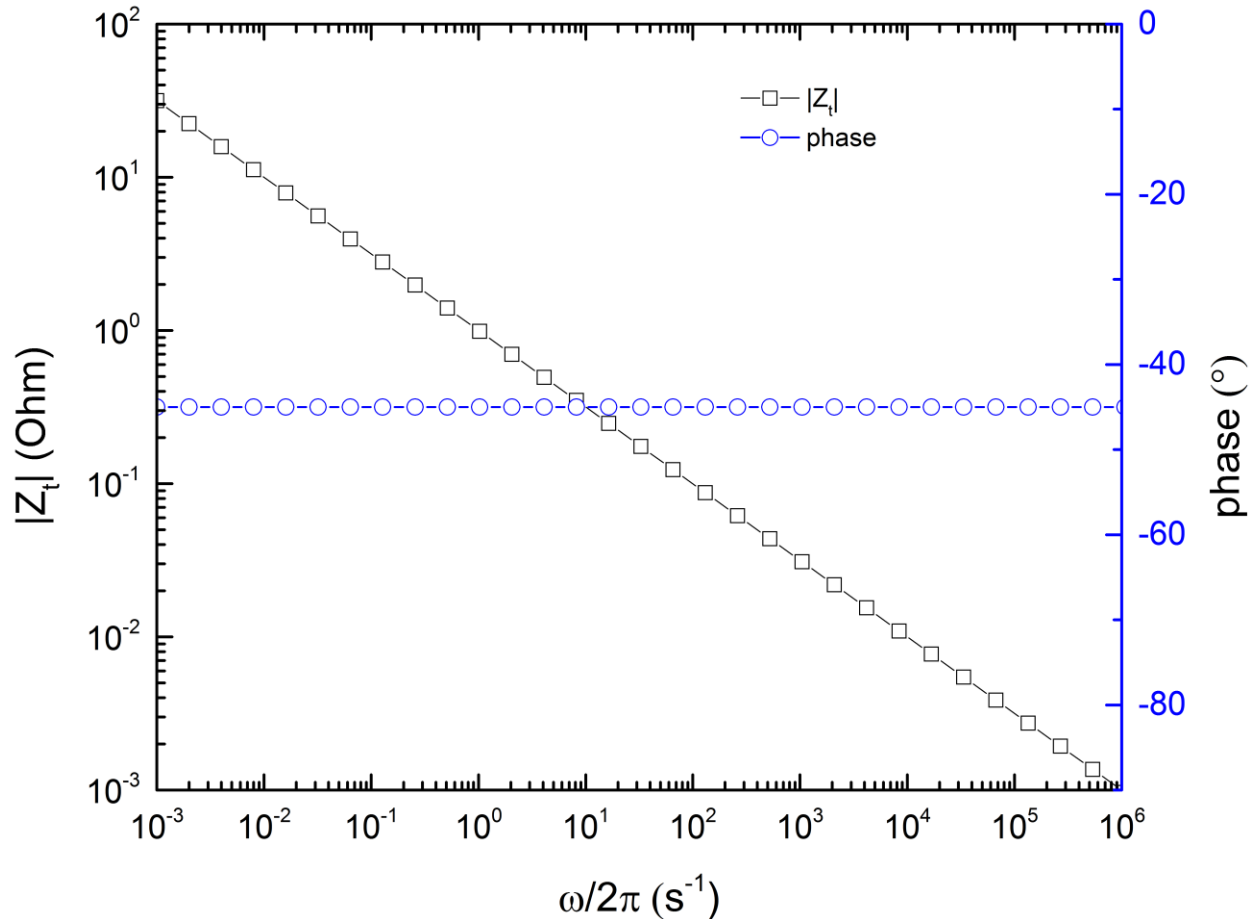


Figure I.3. **The approximate impedance of a elastomer coated with bad electrodes.** The phase angle is at constant  $-45^\circ$  and the absolute value of the impedance decreases as the frequency with an exponent of  $-1/2$ .

Generally the impedance of  $N$  building blocks is described by

$$Z_N = R + \frac{1}{j\omega C + 1/Z_{N-1}} \quad (\text{I.9})$$

This results in a continued fraction of the form

$$Z_N = R + \frac{1}{j\omega C + \frac{1}{R + \frac{1}{j\omega C + \frac{1}{R + \frac{1}{j\omega C + \dots}}}}} \quad (\text{I.10})$$

where the term  $j\omega C$  appears  $N$  times (as does the term  $R$ ). A simplified notation for continued fractions lists only the left part of each denominator such that ( I.10 ) becomes

$$Z_N = (R; j\omega C, R, j\omega C, \dots) \quad (\text{I.11})$$

where the first summand is not a denominator and thus is separated by a semicolon. A second simplification is done by realizing that such an alternating continued fraction can be transformed to a simple continued fraction by

$$Z_N = a (R/a; j\omega C a, R/a, j\omega C a, R/a, j\omega C a, \dots) \quad (\text{I.12})$$

if  $R/a = j\omega C a$  and hence

$$a = \pm R \sqrt{\frac{1}{j\omega RC}} \quad (\text{I.13})$$

Combining ( I.12 ) and ( I.13 ) we get the simple continued fraction with  $2N$  terms

$$Z_N = \pm R \sqrt{\frac{1}{j\omega RC}} (\sqrt{j\omega RC}; \sqrt{j\omega RC}, \sqrt{j\omega RC}, \sqrt{j\omega RC}, \dots) \quad (\text{I.14})$$

A way to evaluate the continued fraction using matrix formulation is

$$(a_0; a_1, a_2, a_3, \dots, a_n) = \frac{h_n}{k_n}$$

$$\begin{pmatrix} h_n & h_{n-1} \\ k_n & k_{n-1} \end{pmatrix} = \begin{pmatrix} h_{n-1} & h_{n-2} \\ k_{n-1} & k_{n-2} \end{pmatrix} \begin{pmatrix} a_n & 1 \\ 1 & 0 \end{pmatrix} \text{ where } \begin{pmatrix} h_{-1} & h_{-2} \\ k_{-1} & k_{-2} \end{pmatrix} = \begin{pmatrix} 1 & 0 \\ 0 & 1 \end{pmatrix}$$

Since we have a pure periodic continued fraction all the  $a_n = \sqrt{j\omega RC}$  and the value of the impedance becomes

$$Z_N = \pm R \sqrt{\frac{1}{j\omega RC} \frac{h_{2N}}{k_{2N}}} \text{ with } \begin{pmatrix} h_{2N} & h_{2N-1} \\ k_{2N} & k_{2N-1} \end{pmatrix} = \begin{pmatrix} \sqrt{j\omega RC} & 1 \\ 1 & 0 \end{pmatrix}^{2N} \quad (\text{I.15})$$

This expression evaluates to (with  $b = j\omega R_0 C_0$ )

$$Z_N = \pm \frac{R_0}{2N} \sqrt{\frac{1}{j\omega R_0 C_0} \frac{(\sqrt{b} + \sqrt{4N^2 + b})^{2N+1} - (\sqrt{b} - \sqrt{4N^2 + b})^{2N+1}}{(\sqrt{b} + \sqrt{4N^2 + b})^{2N} - (\sqrt{b} - \sqrt{4N^2 + b})^{2N}}} \quad (\text{I.16})$$

Taking the limit for  $N \rightarrow \infty$  we arrive at

$$Z_t = \lim_{N \rightarrow \infty} Z_N = \pm \frac{R_0}{\sqrt{j\omega R_0 C_0 \text{Tanh}(\sqrt{j\omega R_0 C_0})}} \quad (\text{I.17})$$

$$\xrightarrow{\omega \ll 1/R_0 C_0} \pm \frac{1}{j\omega C_0}$$

The Bode-Plot for this exact solution is shown in Figure I.4 and clearly shows a cut-off frequency of  $\omega = R_0 C_0$ . At low frequencies the whole system behaves as an ideal capacitor and at high frequencies the system behaves like a capacitor with considerable charge leakage.

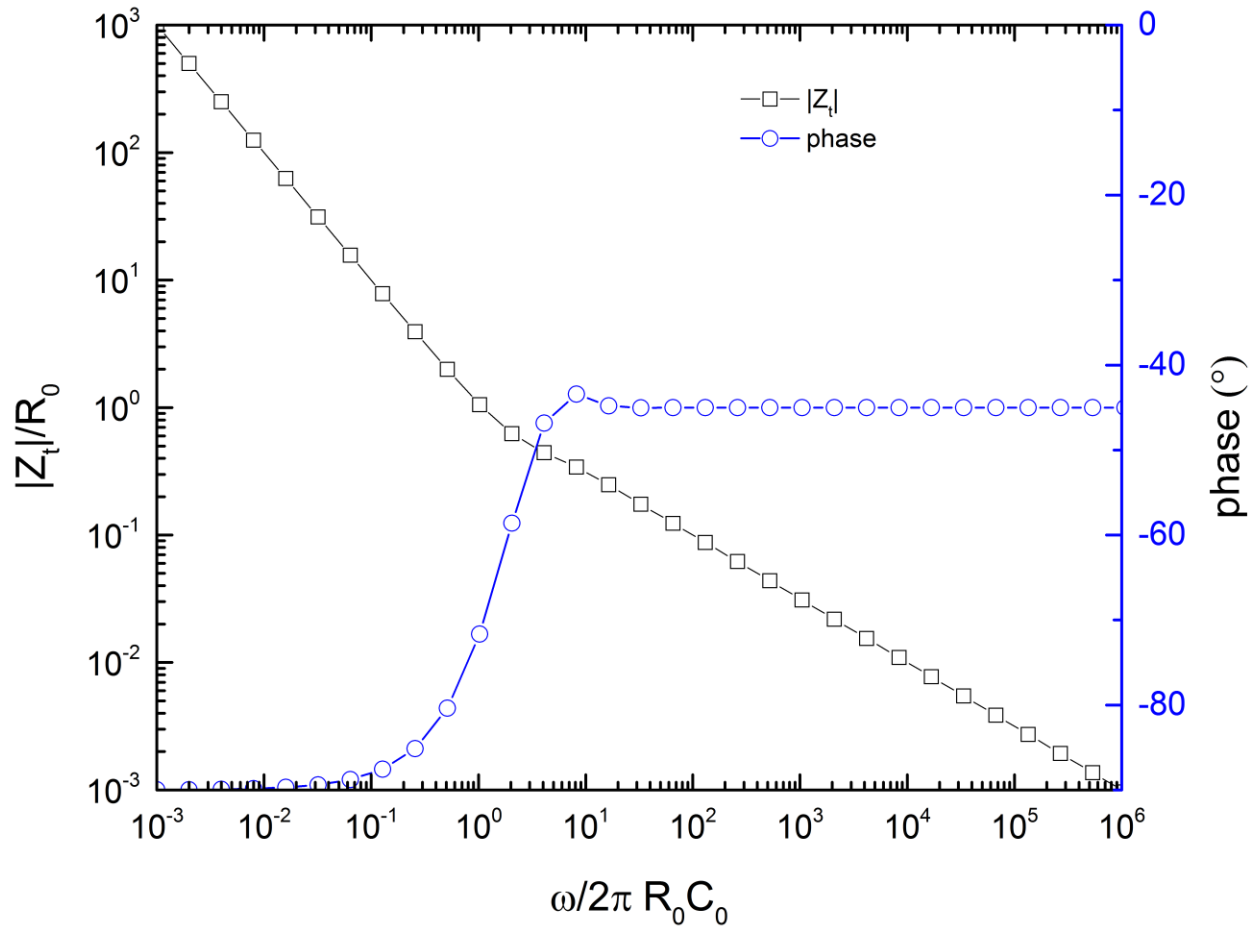


*Figure I.4. The exact impedance of a elastomer coated with bad electrodes. The phase angle changes from  $-90^\circ$  to  $-45^\circ$  and the cut-off frequency is located at  $\omega = R_0 C_0$ . The absolute value of the impedance is  $R_0$  at the cut-off frequency and decreases as the frequency with an exponent of  $-1$  before and  $-1/2$  after the cut-off frequency.*

### I.3. Conclusion

The theoretical analysis of the electrical circuit of an elastomer actuator reveals that below a cut-off frequency of  $\omega = 1/R_0C_0$  the elastomer actuator/generator can be described by an ideal capacitor with capacitance  $C_0$ . Typical values for capacitance  $C_0$  range from  $10^{-12}$  F to  $10^{-7}$  F and for  $R_0$  can under bad circumstance reach  $10^6 \Omega$  resulting in cut-off frequencies of about  $10 - 10^6$  Hz. For frequencies much larger than the cut-off frequency the system is described by

$$Z_t = \frac{R_0}{\sqrt{j\omega C_0 R_0}} \quad (I.18)$$

The charge transferred to and from the elastomer at first glance is expected to be

$$Q_0 = C_0 \Phi$$

At large frequencies the amount of charge changes as the voltage drops at electrode due to higher currents and the impedance changes to  $Z_t$  from ( I.18 ).

This directly translates to a performance loss at operation with high frequencies. A simple solution to avoid this loss mechanism, is to ensure that electrodes are wet and don't dry up, and further limit the operation to lower stretches, where the tendency for percolation is quite low and hence the resistance is kept small. If this is not possible due to the operation constraints one can try to use segmented

actuators with small capacities each, but sufficient capacity and energy density together.

#### **I.4. Outlook and Acknowledgement**

After this theoretical investigation we want to add experimental validation of the above results. This will be of interest to industry and scientific institutions who use and develop dielectric elastomer generators or actuators. As the experiments could not be done in Harvard University due to safety regulations and time-limitations, we will proceed with the experiments at the Johannes Kepler University of Linz. It will be a pleasure to conclude this work and I thank my advisor Zhigang Suo in Harvard and Siegfried Bauer at the JKU for their support and the Austrian Marshall Plan Foundation for funding my stay at Harvard.

## **II. Natural rubber based soft generators enabling sustainable and low-cost energy harvesting**

### **II.1. Introduction**

Current generation technologies cause excessive emission of greenhouse gases and require mining for exotic materials, polluting the environment for decades and putting the well-being of future generations at risk. If polluters are held responsible for their actions it becomes an economical interest to sustainably provide electrical energy. The amount of developable renewable energy resources is significant compared to the annual worldwide production of electrical energy but current technologies yet fail to transduce these resources to electrical energy at competitive price.

Sustainable Natural Rubber (NR) in dielectric elastomer generators (soft generators) availables silent, sustainable, scalable and efficient harvesting of low grade energy such as ocean waves [4], [9], waste heat [10] or human gait [5], [11]. Soft generators using VHB[4], [12–14] or PDMS[15] as working material have been characterized and first prototypes were confirmed to produce electrical power at SRI[16] and SBM[9]. Alternative materials are needed to improve the energy and cost efficiency of soft generators and natural rubber has been suggested for use in soft generators in a theoretical work by Koh et

al[17]. Large scale harvesting of ocean wave energy requires a cheap, sustainable elastomer withstanding high voltages and harsh environmental conditions. In this work we identify NR as a material which is known to endure ocean environment [18], [19], having a small energy and greenhouse gas footprint since its harvested from plants and characterize NR for soft generators, demonstrating high specific electrical energy generated and high specific electrical power in an exemplary conversion cycle. Further we estimate the LCOE of a wave energy converter (WEC) based on soft materials. The estimated levelized cost of electricity (LCOE) of a soft wave energy converter using NR are comparable to that of the LCOE of hydrostatic or geothermal power plants. Commercial harvesting of - otherwise completely unused - energy of ocean waves might be possible using NR due to its low price, supplying strongly needed electrical power.

## **II.2. Wave energy converters**

The energy of ocean wave is huge renewable resource with a global average power of 2 TW [20] or 17 500 TWh which is almost the amount of electric energy generated in 2008 (20261 TWh) [21]. In fact most renewable energy resources are capable of providing as much or even more energy. Details of this analysis is shown in section II.5

Several projects developing wave energy converters (WEC) have been launched to study the feasibility of harvesting energy from ocean waves [22] with some full scale prototypes evolving to promising products [23]. Common to all of these prototypes is a rigid primary structure made of heavy steel or concrete, built to resist the harsh ocean environment including hinges and joints to allow for absorbing the mechanical energy of waves and turbines to convert it into electrical energy.

In order to get over this difficulties two groups proposed to build a soft WEC which resembles PELAMIS [24] but replaces the rigid steel mantle with a soft elastomer[9], [18]. Jean et al.[9] also additionally used dielectric elastomer generators or soft generators to transduce the mechanical energy into electrical energy by stretching a tube made of silicone rubber. This soft generators have been used for wave energy harvesting before by Kornbluh et al. at SRI [4]. The advantage of using soft generators is that they have a very high specific electrical energy generation, there are no moving parts involved, and the output of a soft generators is high voltage direct current which is ideal for long distance transmission in water.

Wave energy is considered one of the most environmentally benign energy sources available [23], but so far no technique is available to harvest wave energy within reasonable costs. Due to harsh environmental conditions in the ocean, heavy weight and size of WECs it is difficult and expensive to maintain offshore wave energy converters like PELAMIS [24], [25]. A

Our estimations show that by using NR as the basic material for soft WECs it is possible to generate low cost electrical energy from waves.

A detailed analysis follows in section II.3 Current state of the art soft generators employ VHB4910™ [4], [5], [14], [26] or silicone rubber [9], [27] as membrane materials reaching specific power outputs of 1 – 120 mW/g. VHB is far too expensive to be used in any large scale application and a soft WEC made of VHB has estimated LCOE of >1\$/kWh. Silicone and natural rubber are provided at lower price and the energy conversion capability of NR is very high.

NR is among the cheapest elastomers available and can be harvested sustainably from plants (rubber trees (*Hevea brasiliensis*) in Brazil and south-east Asia, Guayule (*Parthenium argentatum*) in the USA and Mexico)). It is too stiff to be used in large strain actuators and therefore might have been overlooked for use in soft generators.

Using NR in soft generators allows for harvesting at high specific output power making large scale generation of electrical energy feasible and sustainable at a LCOE ranging from 6.3 – 15.8 ct/kWh.

The describe at what price each kWh of generated electricity by a generator device has to be sold, such that the generator pays back its own cost over the whole lifetime. The LCOE are specific for each technology and energy resource, e.g turbines powered by burning coal have different LCOE from turbines powered by burning natural gas. Evaluating the LCOE requires deep knowledge of technical limits, the jurisdiction which applies (fees, taxes), financial environment (interest rates, availability of capital), government support, public support, and many more [28–30]. Most ocean wave energy generators are based on a rigid structure either-floating or non-floating serving as the wave energy converter (WEC)[31] absorbing the mechanical energy of waves. The absorbed energy is then

converted to electrical energy by a power take off system (PTO), usually a gear-turbine system [22].

A demonstration in wave-tank tests [9], [32] showed that soft WECs can function as a linear-attenuator-type WEC (comparable to PELAMIS and Proteus Wave Power). The soft WEC can also be used as a soft generator[9] as PTO supplying high-voltage DC without the need for additional rigid, moving parts. A soft WEC avoids the need for a separate PTO and substitutes all of the expensive steel structure.

The soft WEC consists of stretchable rubber tube coated with (possibly segmented) compliant electrodes. The whole tube is inflated with water, moored and floats just beneath the water surface. Waves will deform the tube and the deformation is transduced to HVDC using the rubber membrane as soft generator and no additional expensive PTO is needed.

A scheme on how the energy conversion takes place is shown in Figure II.1 and further details are given in section II.9. This design allows for minimizing cost associated with structure of WEC (mostly steel cost), concrete and annual operation and maintenance (OM) which together make up 79% of LCOE as shown in Figure II.2. No active damping is necessary to adjust the resonance frequency of the WEC to the current sea state.

c)

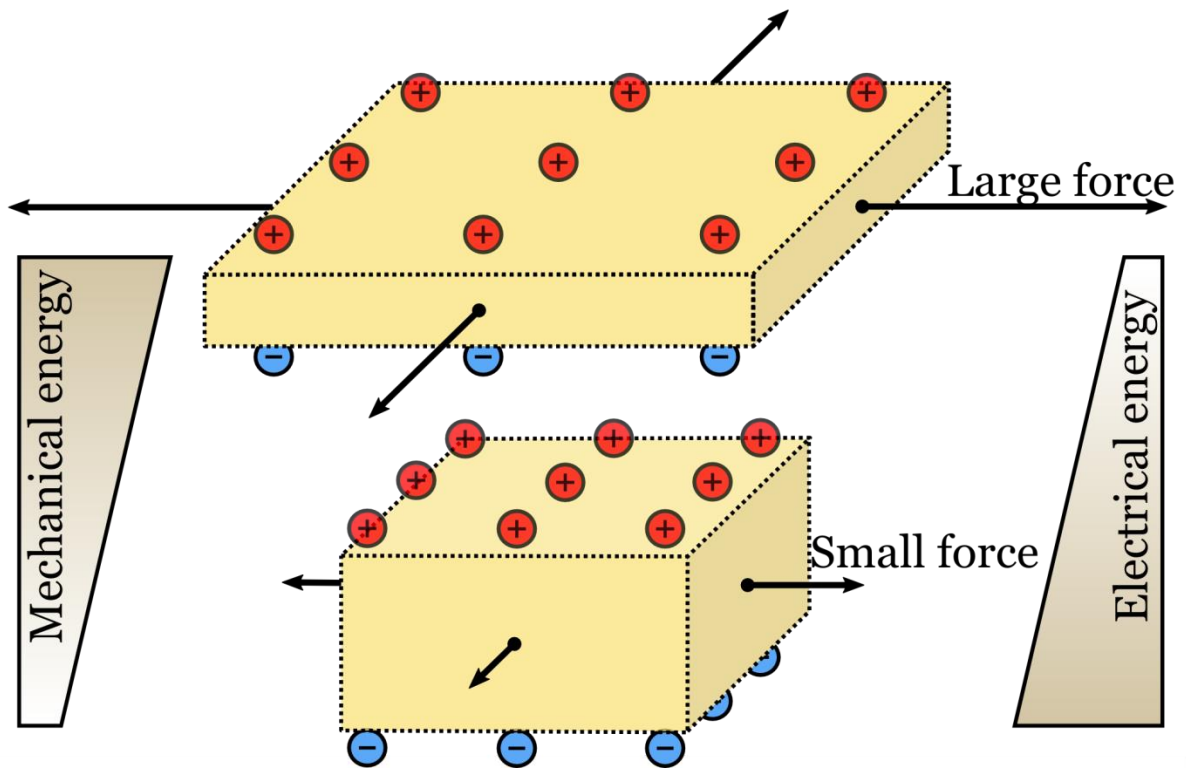


*Figure II.1. Soft generators based on natural rubber turning ocean waves into a source of clean and cheap electricity. Conversion of mechanical to electrical energy with a rubber membrane. Electrical charge  $Q$  is placed on the surface of a stretched rubber membrane. Reduction of stretch forces the electrical charges to move against the electric field, thereby increasing their electrical potential.*

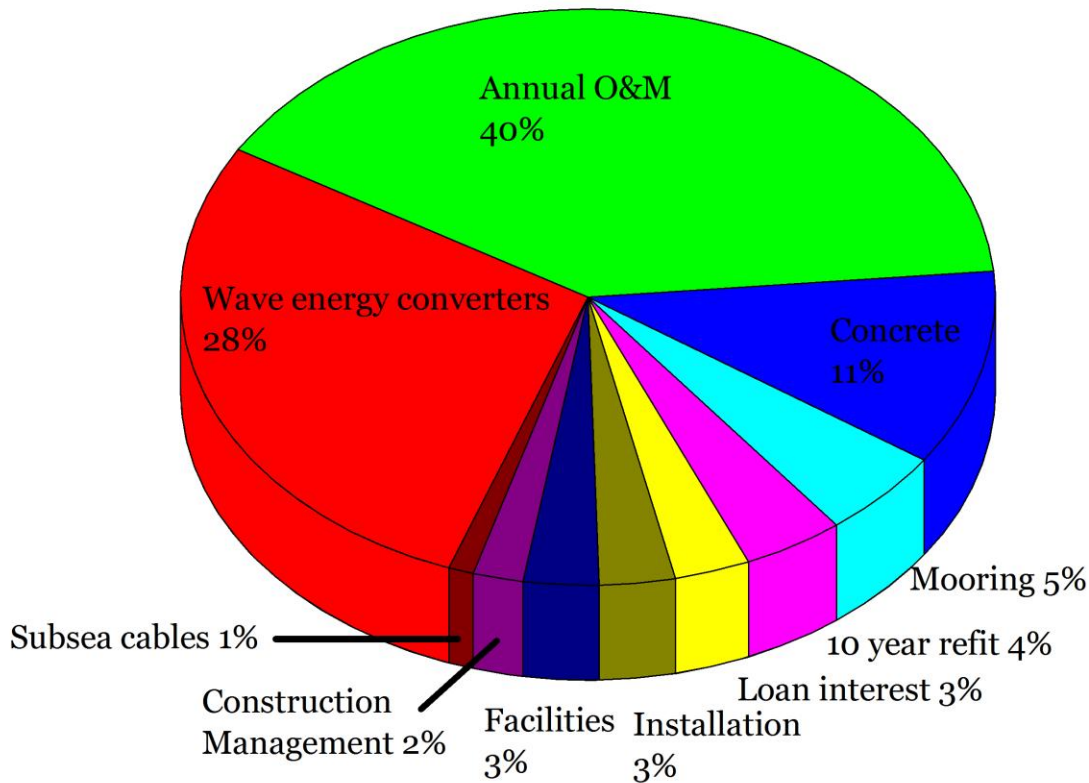


*Figure II.2. Breakdown of levelized cost of electricity for commercial wave energy plant (reproduced from Bedard et al.[25] and CSIRO[33] )*

### II.3. Estimating LCOE

The price for manufactured steel was reported in 2004 to about \$3000/ton[24] and accounting for increased raw steel price (\$650/ton (2004) to \$900/ton (2012)) the manufactured steel price per unit volume in December 2012 is \$33200/m<sup>3</sup> from Previsic et al.[24] converted by raw steel price from December 2004 to

December 2012 ). Elastomers used for soft WEC are VHB4910™ (VHB<sup>1</sup>: \$105000/m<sup>3</sup>), silicone rubber (SR<sup>2</sup>: \$20000/m<sup>3</sup>) and natural rubber (NR[32]: \$7600/m<sup>3</sup>).

Lowering the cost and weight of initial structure also decreases maintenance costs. In contrast to rigid WECs the soft WECs could be moved onto a ship because of their compliance and light weight, possibly allowing for maintenance of multiple WECs simultaneously on the ship. Reducing the number of ships and transfers needed and assuming similar lifetime (up to 25 years according to Farley et al. [32]) we assume a reduction of 20% of the annual cost for O&M compared to rigid WECs. Many rigid WECs have large concrete structures which account for an average of 11% of LCOE. A soft WEC does not contain any concrete and these costs are dropped completely.

In total the LCOE of a soft WEC contain 21% cost unrelated to the materials used (the same as for rigid WEC), 32% O&M (compared to 40% in rigid WECs), 0% concrete cost (compared to 11% in rigid WEC). The material related cost (28% in rigid WECs) scales with its specific average output power ( $P$ ) and its price per volume (\$):

$$\text{LCOE}_{\text{soft}} = \text{LCOE}_{\text{rigid}} \left( 53\% + 28\% \frac{\$_{\text{soft}} P_{\text{Pelamis}}}{\$_{\text{steel}} P_{\text{soft}}} \right)$$

Results for the LCOE using different elastomer materials in a WEC are listed in Table 1. The average power of devices are either

---

<sup>1</sup> Webshop 3M™ for VHB™ Tape 4910 Clear, 12 in x 36 yd 40.0 mil: \$1089.48/Roll ([www.shop3m.com](http://www.shop3m.com) seen at 2013/Mar/06)

<sup>2</sup> Personal Communication with Wattez, Ambroise from SBM Offshore N.V., higher values are reported for small amounts (see Bruzewicz et al.[73] reporting \$70 000/m<sup>3</sup>)

referenced in literature or estimated by to be 1% of the maximal value reported in literature for soft generators (VHB[14]:0.17W/kg, NR(this work): 2W/kg). Even with this safety factor the LCOE are very competitive with other technologies as shown in Figure II.3.

WEC	Average specific power	Material cost	LCOE base on (cent/kWh)			
			CSIRO 2012 <sup>13</sup>	EPRI 2006 <sup>12</sup>	OConnor 2013 <sup>19</sup>	Chu 2012 <sup>20</sup>
PELAMIS (rigid) <sup>3</sup>	3.2 kW/m <sup>3</sup>	33200\$/m <sup>3</sup>	10 - 25	11.6 - 39.1	26.5 - 61.7	29.7 - 79.2
Natural rubber <sup>4</sup>	2 kW/m <sup>3</sup>	7600\$/m <sup>3</sup>	6.3 - 15.8	7.3 - 24.7	16.8 - 39.0	17.7 - 50.1
Silicone rubber <sup>5</sup>	1.1 kW/m <sup>3</sup>	20000\$/m <sup>3</sup>	10.4 - 25.9	12.0 - 40.5	27.5 - 63.9	28.9 - 82.1
VHB <sup>4</sup>	0.17 kW/m <sup>3</sup>	105000\$/m <sup>3</sup>	173 - 432	201 - 676	458 - 1067	483 - 1370

**Table II.i. Material performance, material cost and resulting levelized cost of electricity.**

---

<sup>3</sup> Average Power density reported in McGowin et al. [35]: 153kW at a weight of 380t

<sup>4</sup> Average Power density estimated to be 1% of maximal power density reported (NR this work, VHB Kaltseis et al.[14])

<sup>5</sup> Average Power density reported in Jean et al. [9]:2.8W at a weight of 2.6 kg

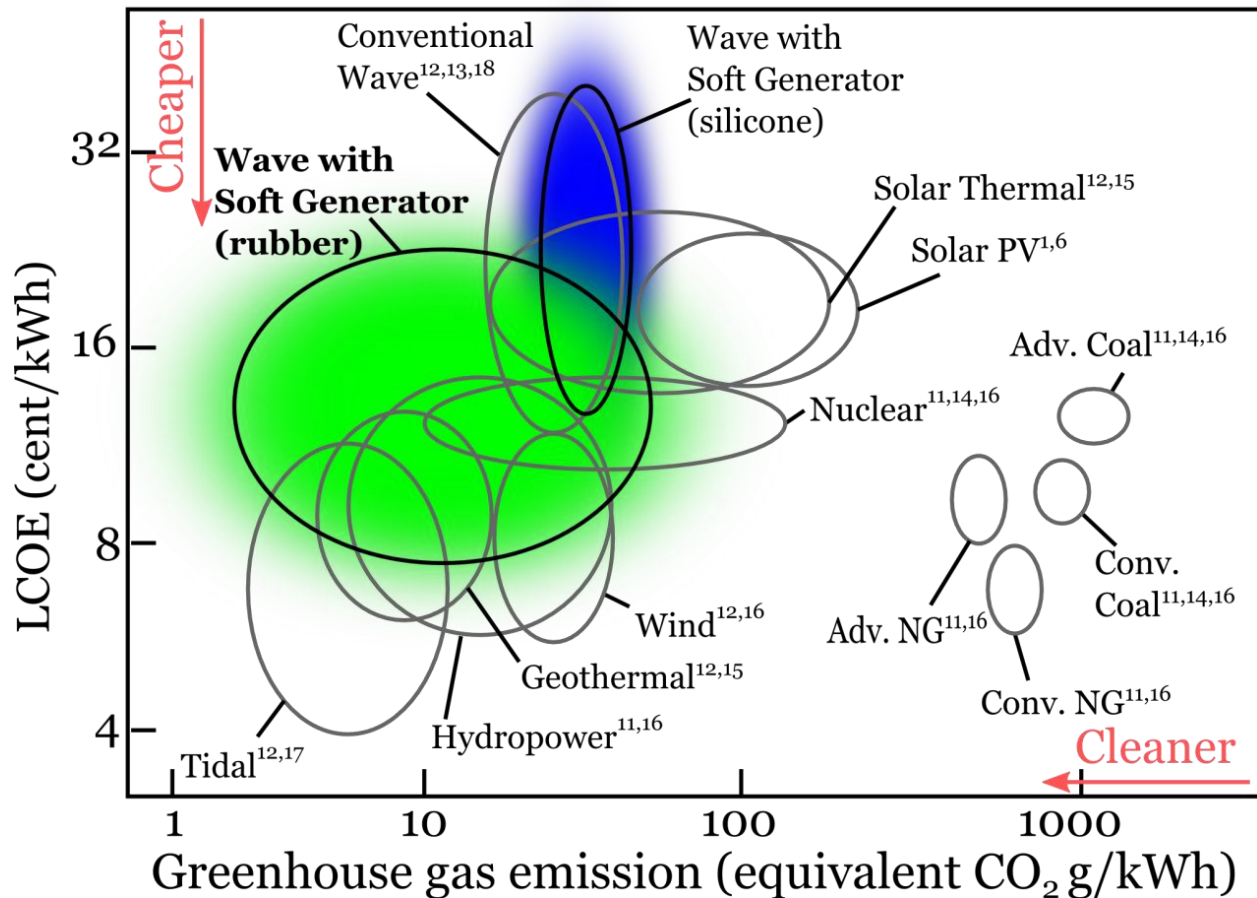


*Figure II.3. LCOE of various energy sources and their greenhouse gas emission. Harvesting energy from ocean waves with existing technology (conventional wave) is a very clean process emitting orders of magnitude less greenhouse gas than fossil fuel based electricity. Currently, high levelized cost of electricity (LCOE) prevents large scale exploitation. Soft generators based on silicone rubber (blue cloud) aim at reducing LCOE. Using natural rubber for soft generators (green cloud) can dramatically reduce LCOE and greenhouse gas emission. [34–43]*

## II.4. Estimating Greenhouse gas emissions

Soft WECs do not produce greenhouse gas (GHG) emissions during operation. For estimating the levelized emission of GHGs (*LGHG*) per generated electricity of soft WECs we consider the emissions during production per ton elastomer (*GHG*) and its average power density (*P*). The levelized emission can be summarized by the following formula:

$$LGHG = \frac{GHG}{P \text{ Lifetime}_{\text{soft}}}$$

We assume equal lifetime of elastomers and steel in seawater (20 years) and consider the reported GHG emissions for NR (GHG of 0.54 – 21 ton CO<sub>2</sub>/ton)[44] and silicone rubber (GHG of 6.3 – 6.6 ton CO<sub>2</sub>/ton)[45]. The resulting LGHG for NR and silicone rubber are 1.5 – 60 g/kWh and 33 – 34 g/kWh respectively. The results of this estimations is visualized in Figure II.3.

## II.5. Potential and Production of Generation of Electricity

Electrical Energy is generated from different primary energy resources such as solar energy, wind energy, geothermal or nuclear energy. Most of these resources are have the potential to provide all the electrical energy needed by the whole world.

The actual energy used to generate electricity on our planet is only a small fraction of the total potential. Almost all resources contribute to the total generation of electricity with a small fraction of their actual potential. An exception is hydroelectric power, which is developed to about 16% and it already becomes increasingly difficult to develop additional projects.

Figure II.4 compares the annual potential and actual annual production of electrical energy of renewable energy resources. Of all resources only tidal energy is not capable of providing a significant amount to the worldwide consumption of electrical energy. This does not mean, that tidal energy is to be neglected since in certain favorable geological locations it can be a very cheap and clean resource. The energy contained in the motion of marine waves is the one large resource not yet exploited on a large scale although it provides electrical energy in a very clean and possibly cheap way.

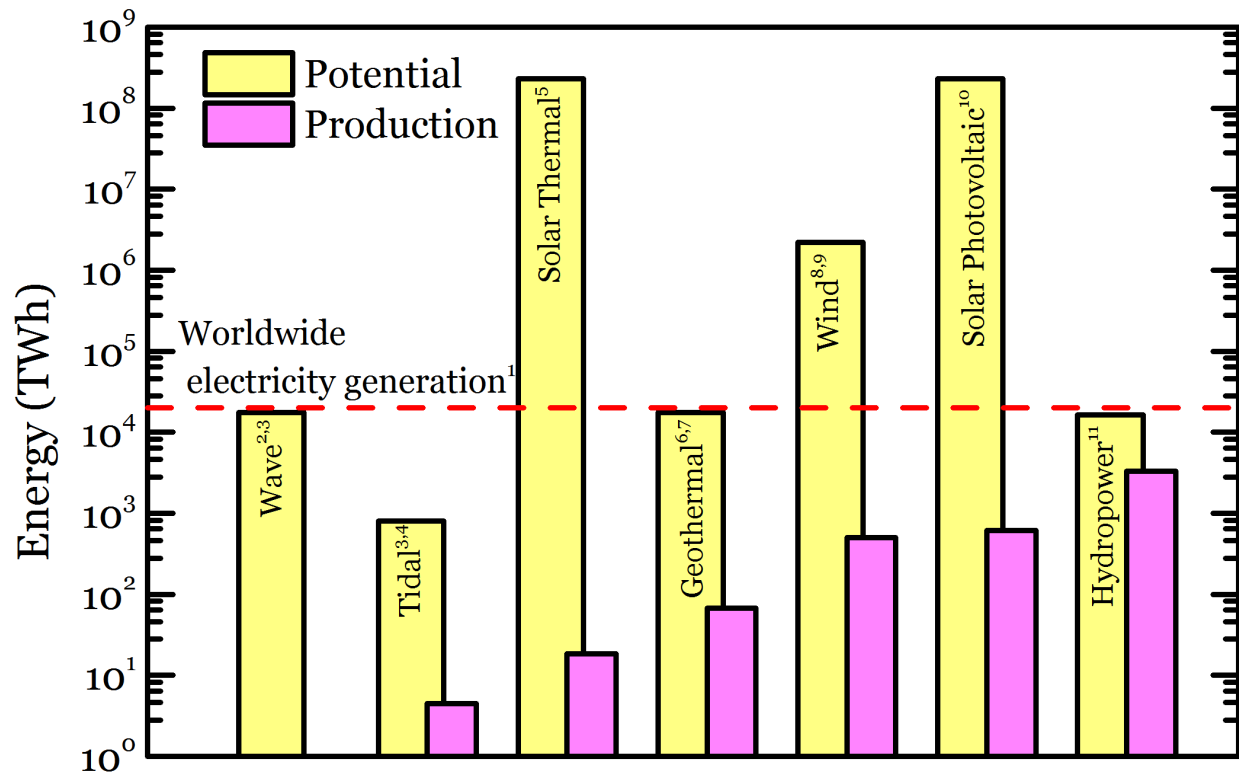


*Figure II.4. The worldwide potential and production of electrical energy from different renewable sources. The annual production of electricity from wave energy is near to zero although the potential is huge (comparable to the potential of hydropower and geothermal and to the total worldwide electricity generation). The red dashed line marks the world consumption in the year 2009.[22], [43], [46–54] The total potential of solar energy was calculated by multiplying the average annual solar irradiation[55] ( $168 \text{ W/m}^2$ ) with a total landmass ( $148 \times 10^6 \text{ km}^2$ ).*

## II.6. Material properties

Three dielectric elastomer materials are characterized throughout this work. ZruElast A1040 (ZRU) from Zrunek GmbH (thickness:  $300 \mu\text{m}$ ) is a natural rubber with unknown filler content which experiences

plastic deformation at large stretches ( $\lambda > 4$ ). Oppo 8003<sup>TM</sup> (OP) from Oppo Medical Inc (thickness: 227 $\mu$ m) is a natural rubber used for physiotherapeutic gymnastic which experiences very small stress-strain hysteresis. VHB4910<sup>TM</sup> from 3M<sup>TM</sup> (thickness: 1000 $\mu$ m) is a polyacrylic foam with very high maximum strain. It exhibits a huge stress-strain hysteresis and is also one of the most used dielectric elastomers for actuators.

The energy yield of a soft generator depends largely on dielectric strength and maximum stretch [56]. It also depends on the dielectric permittivity and the shear modulus. These are the parameters used to assess the aptitude of a material for soft generators.

The mechanical properties of elastomers are well described with the Gent-model[57] . This model has two material parameters which are determined by fitting the model predicted stress-strain curve to experimental data. The first being the small strain shear modulus  $\mu$  and the second is the limiting stretch  $J_{lim}$ . The free energy increment of a soft generator with respect to increments of the charge  $dQ$  or the strain in direction  $d\lambda_i$  is [58]

$$dF = \phi dQ + V \frac{\partial W_{Gent}}{\partial \lambda_i} d\lambda_i \quad (\text{II.1})$$

With

$$W_{Gent}(\lambda) = -\frac{\mu J_{lim}}{2} \ln \left( \frac{J_{lim} - (\lambda_1^2 + \lambda_2^2 + \lambda_3^2 - 3)}{J_{lim}} \right) \quad (\text{II.2})$$

Most elastomers are incompressible and for uniaxial tensile deformation this means that  $\lambda = \lambda_1 = \lambda_2^{-2} = \lambda_3^{-2}$ . The model predicts a uniaxial nominal stress – strain response of

$$s = \frac{P}{A_0} = \frac{1}{A_0} \frac{dF}{dL} = \frac{dF}{V d\lambda} = \frac{\mu J_{lim}(1 - \lambda^3)}{\lambda^2(J_{lim} - \lambda^2 - 2\lambda^{-1} + 3)} \quad (\text{II.3})$$

Eq. (II.3) is fitted to experimental stress-strain data within good agreement as shown in Figure II.5a. The material parameters for OP and ZRU are typical for natural rubbers and the shear modulus of VHB is typically an order of magnitude lower than that of NR while its limiting stretch is very large.

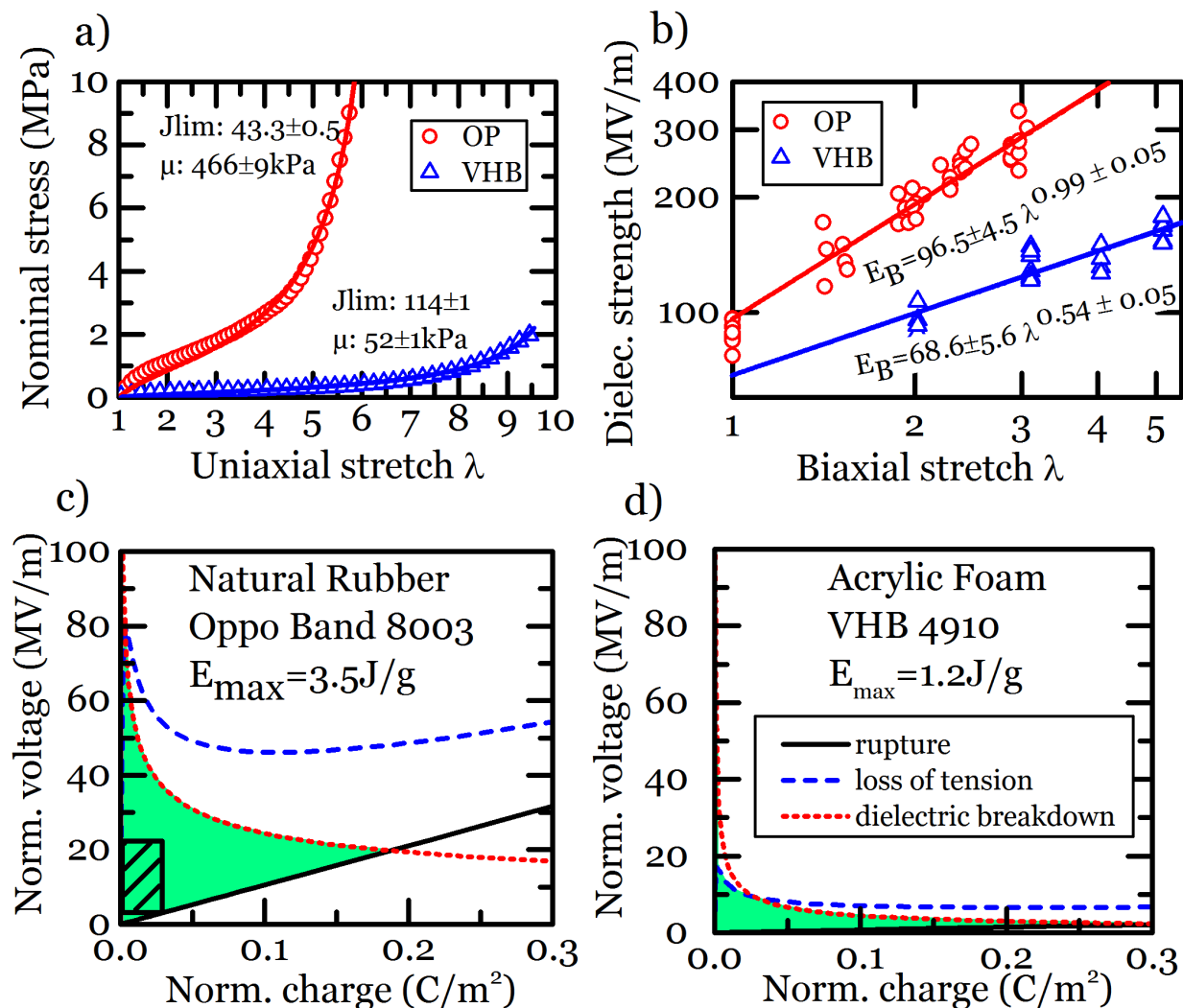


Figure II.5. **Favorable material properties of natural rubber (Oppo Band 8003) for soft generators compared to the commonly used acrylic elastomer (VHB4910).** a) Nominal stress-stretch relations fitted to a Gent-Model for VHB (blue triangles) and Oppo Band (OP) (red circles). b) The dielectric strength of NR is significantly higher compared to VHB, especially at larger stretches. c-d) Material limits (rupture, loss of tension and dielectric breakdown) enclose an area (green) of safe operation states for soft generators. The green area defines the maximum specific electrical energy that can be generated per cycle. The shaded part within the green area in c) depicts the experimental generator cycle reported in this work.

Good performance of soft generators is possible with natural rubbers in general. To make this claim plausible we assess the aptitude of a natural rubber (ZRU) whose filler material differs from that of OP. The mechanical and electrical properties of ZRU are compared to OP in Figure II.6.

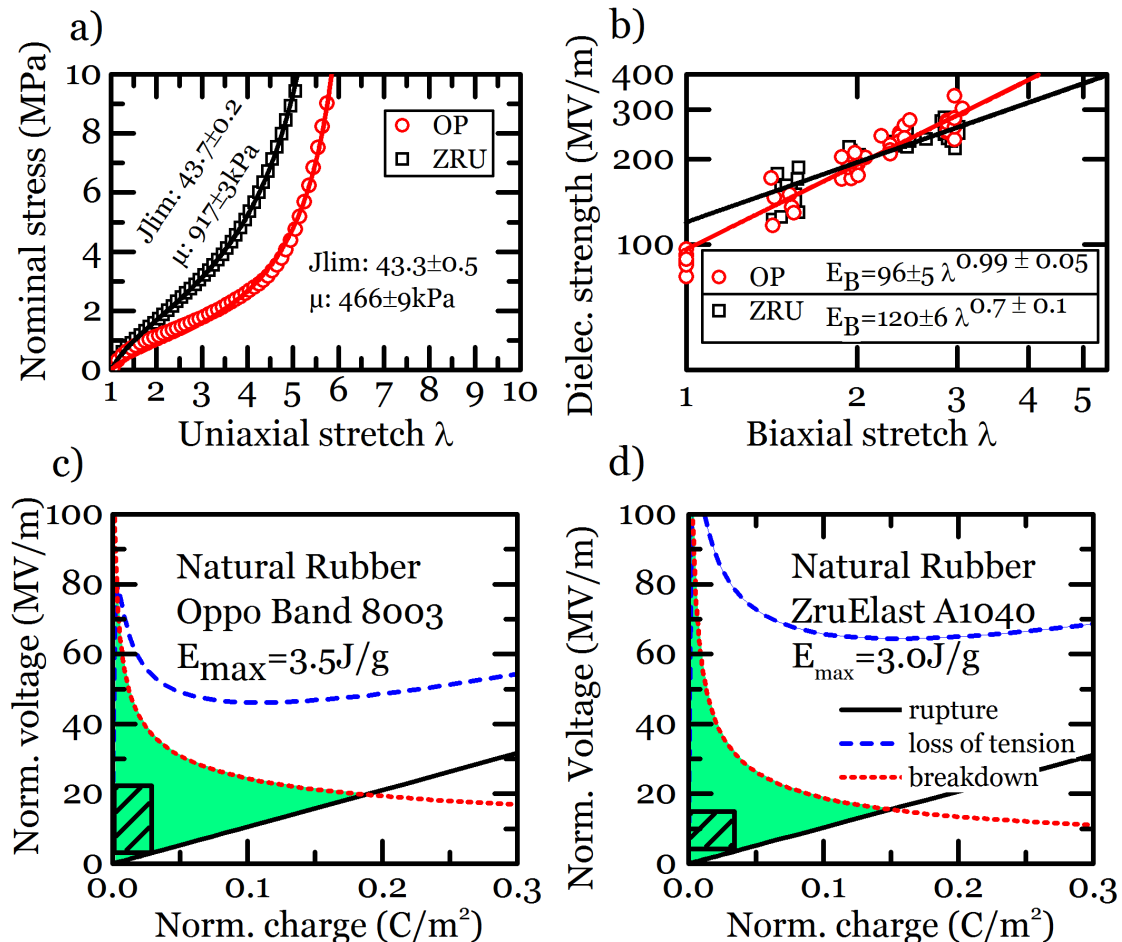


Figure II.6. **Mechanical and electrical properties of ZruElast A1040.** a) The shear modulus of ZRU doubles that of OP but the maximum stretch is very similar. b) At low stretches ZRU has superior dielectric strength compared to OP. The dielectric strength grows slower in ZRU and thus at high stretches OP shows higher durability to electric fields. c-d) As ZRU and OP have quite similar mechanical and electrical properties, the achievable energy yield per cycle is similar. The shaded areas denote the experimental harvesting cycles shown in this work.

The different filler material of ZRU seems to have a negative effect on its dielectric strength and causes plastic deformation. Nevertheless its performance in a soft generator is comparable to that reported for VHB and PDMS.

The electrical material parameters of elastomer are dielectric strength  $E_B$  and permittivity  $\epsilon_r$ . The relative permittivity of OP and ZRU are  $\epsilon_r = 2.7$  and  $\epsilon_r = 3.2$  respectively with a very weak stretch dependence. The relative permittivity of VHB4910<sup>TM</sup> is  $\epsilon_r = 4.2$  which agrees with values reported in literature [59], [60].

Application of an electric field to an elastomeric membrane leads to actuation[61] which in a clamped sample will develop inhomogeneous deformation. The intrinsic dielectric strength is measured with small area electrodes and local thickness variations due to inhomogeneous deformation make it very hard to determine the electric field. We measure the dielectric strength of NR and VHB while preventing actuation during application of voltage (method submitted [62]). In Figure II.5b and Figure II.6b the stretch dependence of the dielectric strength is fitted to a simple power law

$$E_B(\lambda) = E_0\lambda^R$$

The dielectric strength of OP is exceptionally high compared to that of VHB at high stretches. At low stretches ZRU exhibits the highest dielectric strength.

Figure II.5 and Figure II.6 c-d compare the area of allowable states of an equal-biaxially stretched OP, ZRU and VHB in the electrical work-

conjugate plane  $\phi/H_0 - Q/A_0$  where  $\phi/L_0$  is the normalized voltage applied through a membrane of thickness  $H_0$  and  $Q/A_0$  is the normalized charge on that membrane with an area of  $A_0$ . The failure modes of a material are borders to the region of allowable states in a work-conjugate plane. Any state characterized by a point outside this area leads to immediate failure and destroys the material. Rupture happens at the maximum strain which is defined by

$$2\lambda_{max}^2 + \lambda_{max}^{-4} - 3 = J_{lim} \quad (\text{II.4})$$

Charging the soft generator at maximum strain is described by a straight in the voltage-charge plane described by

$$\frac{\phi_{rupt} \left( \frac{Q}{A_0} \right)}{H_0} = \frac{Q}{A_0} \frac{1}{\varepsilon_0 \varepsilon \lambda_{max}^4} \quad (\text{II.5})$$

Breakdown occurs, whenever an electric field larger than the dielectric strength is applied through the membrane thereby destroying it. The limiting curve of dielectric strength in the voltage-charge plane is given by

$$\frac{U_{break} \left( \frac{Q}{A_0} \right)}{H} = E_0 \left( \frac{1}{\varepsilon E_0} \frac{Q}{A_0} \right)^{\frac{R-2}{R+2}} \quad (\text{II.6})$$

If subject to voltage, an elastic membrane deforms even without stress being applied [58]. Under clamping conditions this leads to loss of tension where no mechanical energy is stored in the membrane and hence no energy conversion can take place. The

limiting curve of loss of tension is determined numerically from the condition that the nominal stress  $s = 0$ .

The high shear modulus of ZRU and OP result in high voltages for the loss of tension limit which is in contrast to applications for actuation where a low shear modulus is favorable to produce high strain. The high dielectric strength of NR further improves its theoretical performance. For this reasons the theoretical specific energy per cycle is 3 times larger for NR than for VHB. Viscoelastic effects in NR are very small which allows for operating a soft generator and much higher frequency than with VHB. Further the similarities between OP and ZRU indicate, that the filler materials do not change the total behavior too much and that NR generally is a good material for soft generators.

The high maximum stretch of VHB lowers the rupture limit which is the lower boundary of the region of allowed states. This might not be exploited in applications aiming for high life time. Applied electric fields in a cycle should be at the most 33% of the intrinsic dielectric strength of a material to operate in a safe regime and even less to extend the lifetime of a soft generator.

## II.7. Determination of fracture energy

To assess the durability of the materials the fracture energy is measured with a method proposed by Rivlin and Thomas [63]. A high fracture energy indicates that a large amount of mechanical energy can be absorbed by the material without failure. This has two positive effects since it increases the lifetime and the energy density due to the high absorption capability.

The fracture energy is defined as the mechanical energy required to propagate a pre-existing crack [63]. A wide and short sample of dimensions  $L$  and  $H$  was clamped along the long edge (Figure II.7). A pristine sample and a sample with a precut were separately stretched to rupture. The fracture energy ( $\Gamma$ ) is computed as:

$$\Gamma = W(\lambda_{rup}) \times H \quad (\text{II.7})$$

where  $\lambda_{rup}$  denotes the rupture stretch of the precut sample. The mechanical energy density  $W(\lambda)$  is obtained from the area under the nominal stress-stretch curve of a pristine sample.

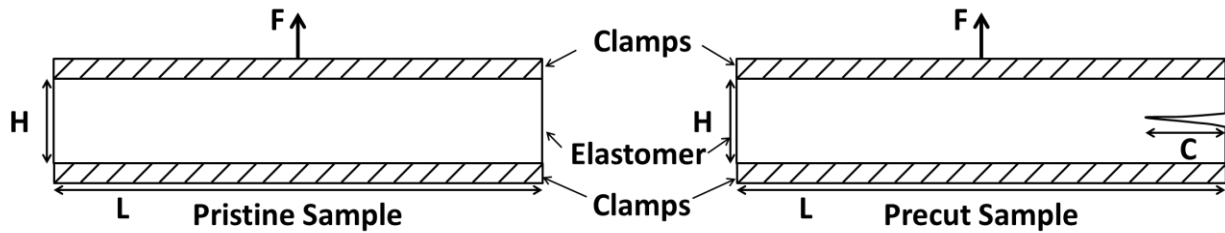


*Figure II.7. Schematic of samples prepared for fracture energy determination.* A ZWICK Universal Testing Machine was used to obtain the experimental nominal stress-stretch curves for the samples. The dimensions of the samples are:  $L = 100$  mm,  $H = 10$  mm for VHB 4905 and 15mm for Zrunek and OppO rubber. The thicknesses of the samples are: 0.5 mm for VHB 4905, 0.3 mm for ZruElast<sup>TM</sup>A1040 and 0.227 mm for OppO 8003 rubber. Samples are stretched at three strain rates: 1%/s, 10%/s and 100%/s.

Stress stretch curves of pristine samples were obtained for the three strain rates (1%/s, 10%/s, 100%/s). For each rate, 3 samples are tested for VHB and 5 samples are tested for ZRU and OP. The experiments show that VHB 4905 exhibits strain-rate-dependence in its stress-stretch response, as shown in Figure II.8. On the other hand, the stress-stretch response of both rubbers (ZruElast and Oppo) appear to be independent of strain rate.

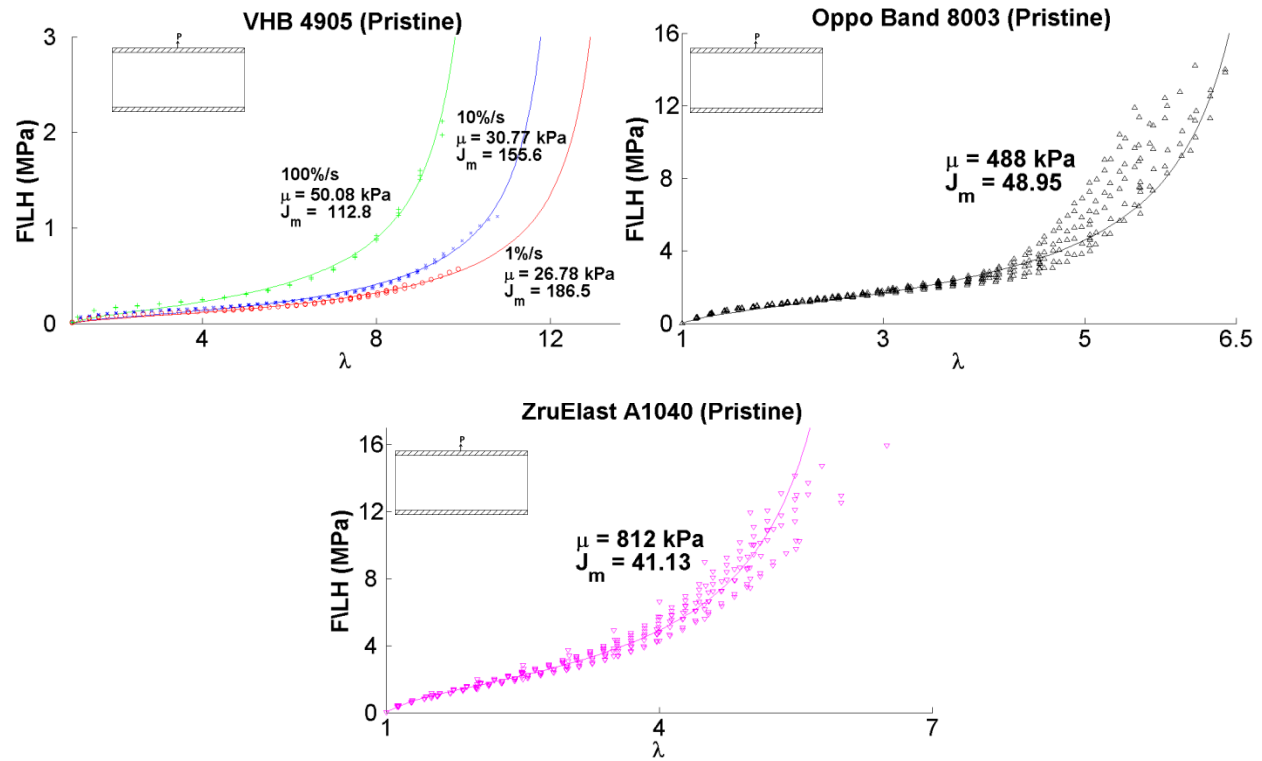


**Figure II.8. Experimental nominal stress-stretch data of pristine samples fitted to the Gent model**

The experimental data was fitted to the Gent model[57] for pure shear deformation ( $\lambda = \lambda_1 = \lambda_3^{-1}; \lambda_2 = 1$ ) giving the mechanical energy density function as follows (resembling (II.2)):

$$W = -\frac{\mu J_{lim}}{2} \ln \left( 1 - \frac{\lambda^2 + \lambda^{-2} - 2}{J_{lim}} \right) \tag{II.8}$$

The relationship between force  $F$ , and stretch  $\lambda$  is given by the equation-of-state:

$$\frac{F}{LH} = \frac{dW}{d\lambda} = \frac{\mu(\lambda - \lambda^{-3})}{1 - \frac{\lambda + \lambda^{-2} - 2}{J_{lim}}} \quad (II.9)$$

The analytical fit to the experimental data is then used to compute the mechanical energy density of each material. The precut samples were similarly stretched at the three strain rates. Figure II.9 shows that VHB has a much larger rupture stretch as compared to both rubbers. This is expected as VHB sustains a much larger stretch in its pristine state, as compared to both rubbers.

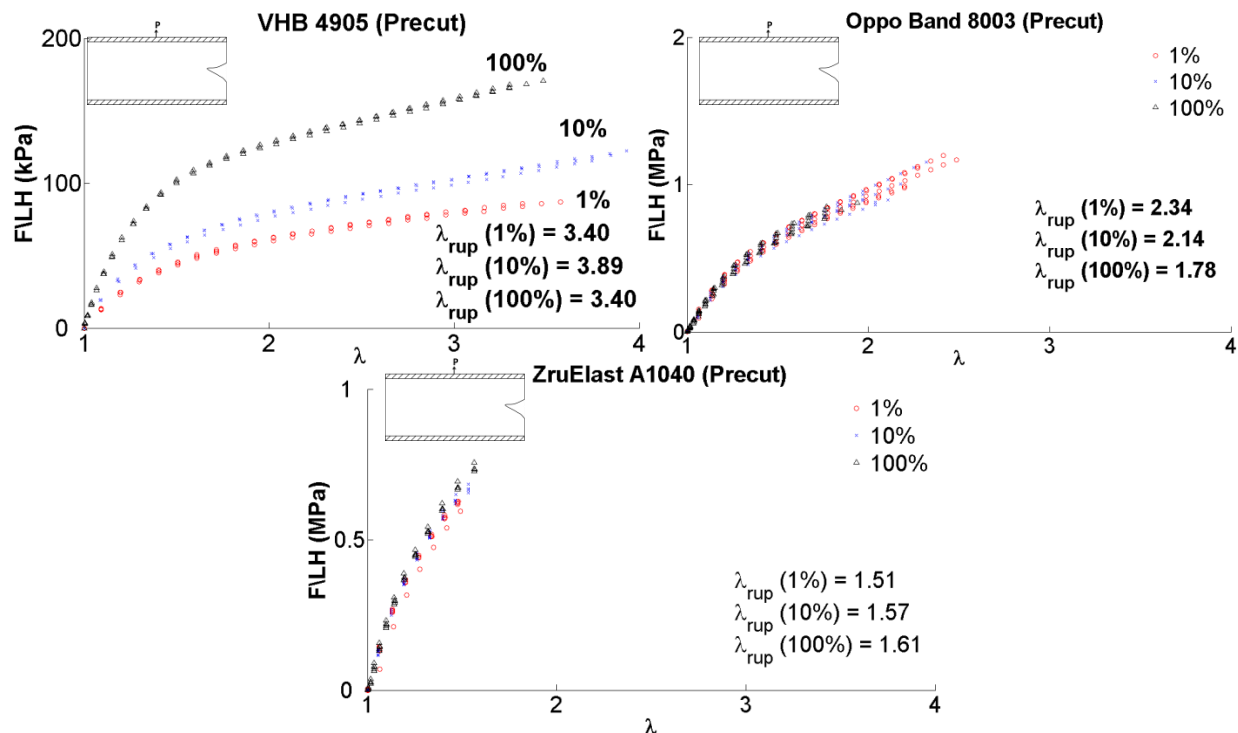


Figure II.9. **Rupture stretches of precut samples.** The data obtained from Figure II.7 and Figure II.8 were put into equation (1), and the fracture energies for all elastomers were summarized in Table II.ii below.

Strain rates (%/s)	VHB (kJ/m <sup>2</sup> )	ZruElast™A1040 (kJ/m <sup>2</sup> )	OppO 8003 (kJ/m <sup>2</sup> )
1%	1.99	4.45	16.86
10%	3.33	5.42	13.07
100%	3.92	6.15	7.21

*Table II.ii. Fracture energy of elastomers.*

It is observed that the fracture toughness of rubber is much higher than VHB, with a maximum of 8.5 times for OppO rubber compared to VHB at a strain rate of 1%/s. The fracture energy for VHB is consistent with a previously reported result[64]. It has been shown in previous works that the fracture energy of amorphous polymers is correlated with its fatigue life against cyclic loading[65]. We may hence conclude that both rubbers are more durable against cyclic operation than VHB.

## **II.8. Hysteresis loss for elastomers**

When an elastomer undergoes a mechanical cycle of loading and unloading, the unloading path is typically different from its loading path. When plotted on a stress-strain plane, the resulting area traced by the loading-unloading cycle gives a measure of the amount of mechanical energy lost due to viscous effects, known as the hysteresis loss. We obtain hysteresis losses for samples of acrylic-based VHB, and natural rubber-based ZRU and OP, by an experiment of cyclic loading and unloading. Samples are uniaxially stretched to a

prescribed maximum nominal strain of 200%, at a prescribed strain rate of 5%/s, and then unloaded at the same strain rate. This loading-unloading process was repeated 100 times for each sample. The 100<sup>th</sup> cycle is plotted in Figure II.10 to illustrate the relative hysteresis losses for each material.

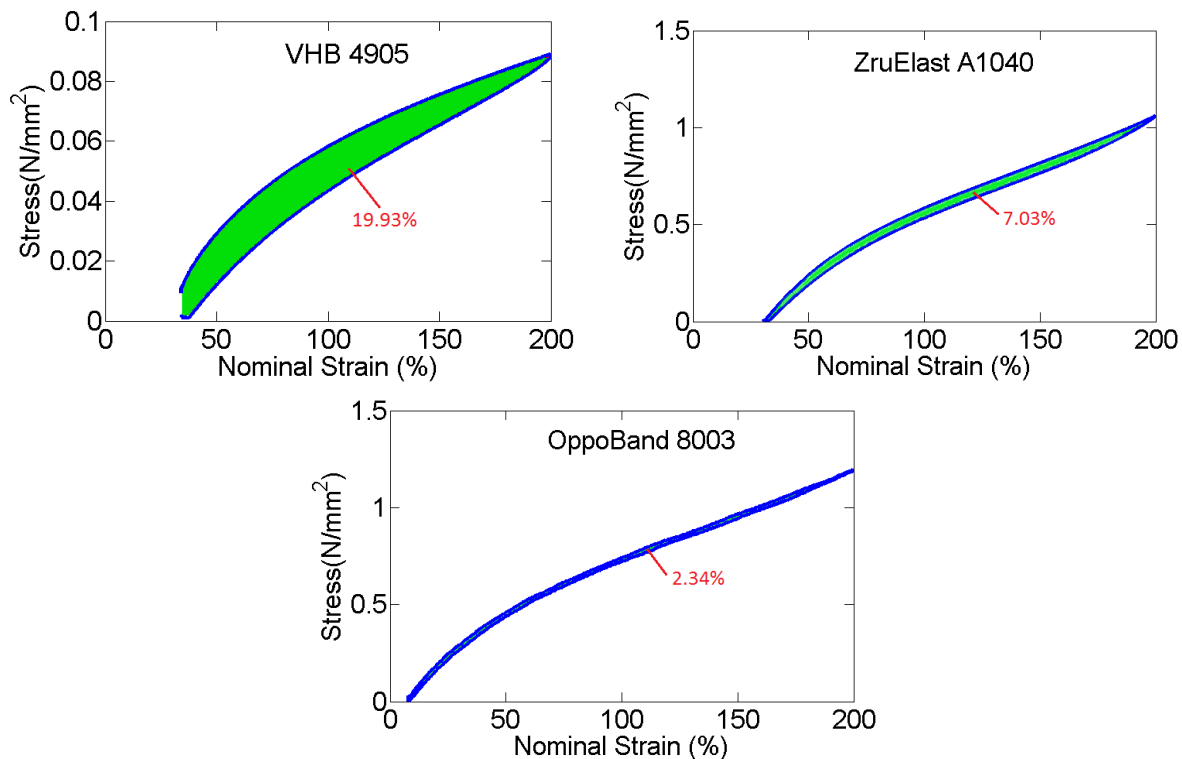


**Figure II.10. Hysteresis for VHB 4905, ZruElast A1040 & OppoBand 8003.**

Hysteresis loss is expressed as a percentage of total mechanical energy stored during loading. The non-zero initial strain before loading indicates some residual strain in the material accumulated over previous cycles. This experiment shows that natural rubber-based ZRU and OP give lower hysteresis losses compared with acrylic-based VHB, with OP displaying the lowest loss at 2.3%. OP

also displays best performance in terms of strain recovery, with a residual nominal strain of about 8% after 100 cycles, compared with 35% for ZruElast and 40% for VHB. This implies that OP is most efficient in mechanical cycling, displaying nearly perfectly elastic behavior over a nominal strain of 200%.

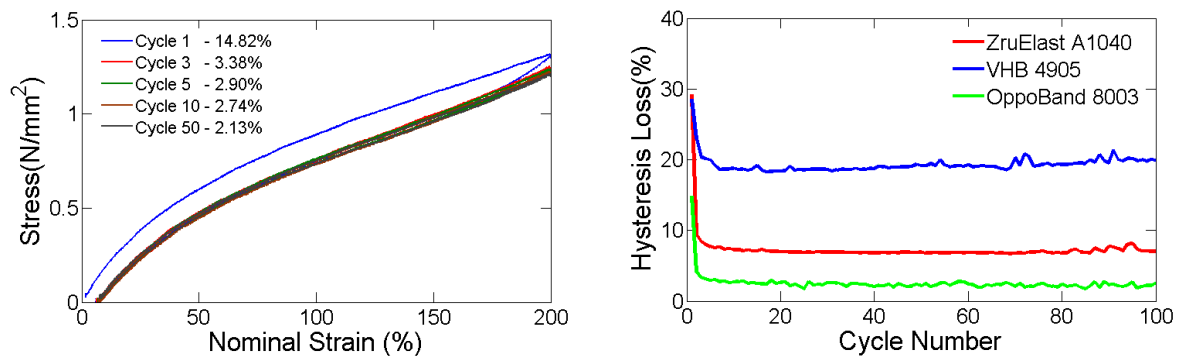


**Figure II.11. Steady-state hysteresis loss**

Figure II.11 compares the hysteresis for cycles 1, 3, 5, 10 and 50 for OppoBand, and the hysteresis loss over the 100 cycles for all three materials. All of them exhibit large hysteresis losses in the first cycle, which gradually saturates to a lower value from the 5<sup>th</sup> cycle onwards. This may be attributed to the Mullins effect[66], [67]. Mullins Effect is the irreversible softening of an elastomer filled with carbon black fillers, first proposed by Leonard Mullins, which theorizes that an elastomer with carbon fillers irreversibly softens after each cycle of loading-unloading. Its effect is most observable in the first few stress cycles of a virgin elastomer, and gradually diminishes for subsequent cycles. In the above figure, steady-state is defined as the cycles beyond the initial rapid drop in hysteresis loss for all elastomers.

## II.9. Energy conversion

The mechanism of energy conversion in a soft generator is sketched in Figure II.12. Figure II.12a shows the exemplary cycle realized by the circuit shown in Figure II.12b. Prior to starting the conversion cycle, the input and output capacitors are charged to low and high voltage respectively. Charges are extracted from the input capacitor while the soft generator is stretched as the voltage of the membrane and the input capacitor equalize. Upon relaxing, the generator boosts the voltage until it matches that of the output capacitor when it starts to discharge. By stretching the generator the voltage drops until the initial state is recovered.

High mechanical energy is stored in the soft generator when applying large stretching forces (Figure II.12c left). The electrical energy stored is  $Q^2/2C$  and is low for a state with large capacity due to large area and small thickness. As the stretching force decreases the soft generator contracts (Figure II.12c right) and mechanical energy is converted by doing electrical work through decreasing the capacity of the soft generator while the charge is kept constant. This basic operations, namely charging/discharging and stretching/relaxing are used to create a cyclic process to generate continuous high voltage direct current. In this work the soft generator is realized by a elastomer membrane which is inflatable to balloon shape. The mechanical work consumed by changing the volume of the soft generator is

$$W_{mech} = \int p dV \quad (\text{II.10})$$

with the work-conjugate variables pressure  $p$  and volume  $V$  of the balloon. The useful electrical work done by the soft generator by charging and discharging the capacitors is

$$W_{net} = \int \phi dQ_{out} - \int \phi dQ_{in} = \int \phi dQ_{net} \quad (\text{II.11})$$

where  $dQ_{out}$  and  $dQ_{in}$  refer to the amount of charge transferred to/from the output/input capacitor. A charged and stretched dielectric elastomer membrane is a compliant variable capacitor storing mechanical as well as electrical energy. The basic operations for a soft generator using balloons are charging/discharging and inflation/deflation.

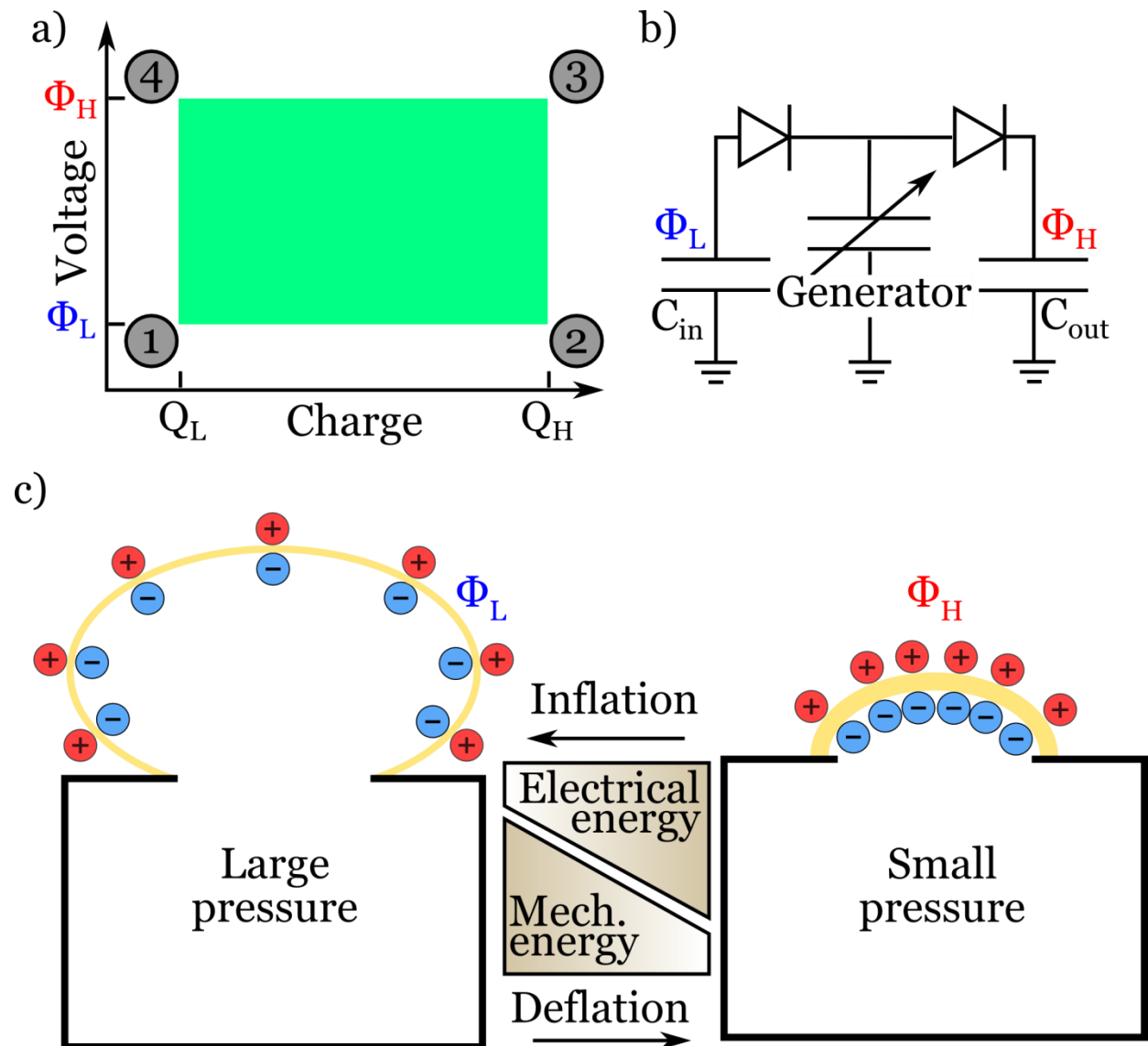


Figure II.12. **Experimental design of a soft generator based on charge reservoirs of low and high potential.** Balloon inflation is used to provide mechanical energy. a) A rectangular, Carnot-inspired cycle in the voltage-charge plane is chosen for the generator. b) The soft generator operates between reservoir capacitors at low ( $\Phi_L$ ) and high ( $\Phi_H$ ) potential. Diodes direct charges on the generator to be pumped from low to high potential. c) Pressurized air is used to deform the elastomer membrane (yellow) into a balloon shape. Deflation of the balloon converts stored mechanical energy into electrical energy.

Before generation the reservoirs are charged to the desired input and output voltages. The generator is charged to match the voltage of the input reservoir due to connection via the diode marking point 1. At this stage the cyclic generation starts. Upon inflation (step 1- 2) charge is transferred to the generator from the input reservoir while the voltage is held constant because the charge transferred to the generator is small compared to the total charge stored. After maximum dilation of the generator (point 2) its capacity shrinks and the voltage rises and the diode passively disconnects the generator from the input reservoir. When the generators voltage matches the voltage of the output reservoir it becomes connected (point 3) and the generator discharges (step 3-4) while the generator reaches minimum dilation at point 4. By stretching the generator again the voltage drops and the output reservoir becomes disconnected. When the voltage of the generator dropped to the voltage of the input reservoir one full cycle is concluded at point 1 and the generator is ready to engage in the next cycle.

## **II.10. Modelling of Balloon Deformation**

Charges are only exchanged with the reservoirs during charging (step 1-2) and discharging (step 3-4). The reservoirs used in the experiment are finite therefore transferring charge to and from the reservoir

results in a voltage rise and drop respectively. The voltage drop/rise during this steps is used to calculate the net-charge  $Q_{net}$  by eq.(5).

This method is used to evaluate the capacity as a function of volume of the inflated membrane. The capacity changes over two-orders of magnitude due to the unequal biaxial stretch and a comparison to the numerical simulation of this process shows very good agreement with the experiment (see Figure II.13a).

Because the edge of the rubber membrane is clamped by the chamber, the membrane undergoes inhomogeneous deformation as it expands into a balloon. The apex of the membrane is under equal-biaxial stretching, while the edge of the membrane is under unequal-biaxial stretching. The inhomogeneous deformation has been previously analyzed and solved by considering a nonlinear boundary-value problem [68–70].

We adopt the model of ideal dielectric elastomers, where the Helmholtz free energy contains the elastic energy due to the stretching of the elastomer and the electrostatic energy due to polarization of the elastomer[71]. Specifically, the electric displacement  $D$  is linear in the electric field  $E$ , and the permittivity  $\varepsilon$  is independent of deformation, such that  $D = \varepsilon E$ . At large deformation, the elastomer exhibits stiffening. To model this effect within the Gent-Model we describe the Helmholtz free energy density as:

$$W(\lambda_1, \lambda_2, D) = -\frac{\mu J_{lim}}{2} \ln \left( 1 - \frac{\lambda_1^2 + \lambda_2^2 + \lambda_1^{-2} \lambda_2^{-2} - 3}{J_{lim}} \right) + \frac{D^2}{2\varepsilon} \quad (\text{II.12})$$

where  $\lambda_1, \lambda_2$  are the stretches in radial and circumferential direction respectively,  $D$  is the electric displacement, and  $\varepsilon$  is the permittivity. In writing ( II.12 ), the elastomer is assumed to be incompressible, such that  $\lambda_1\lambda_2\lambda_3 = 1$ . The first term in ( II.12 ) represents the elastic energy by the Gent model[57].

The free energy of the membrane is an integral over the area of the membrane  $\int W dA$ . When the volume of the balloon varies by  $\delta V$ , the pressure  $p$  excess to the atmospheric pressure does work  $p\delta V$ . When the charge on either electrode varies by  $\delta Q$ , the voltage does work  $\phi\delta Q$ . The balloon achieves an equilibrium state when the variation of the free energy of the membrane equals the combined work done by the pressure and the voltage:

$$\delta \int W dA = p\delta V + \phi\delta Q \quad (\text{II.13})$$

The equilibrium condition leads to a set of differential equations; exact forms of these equations may be found in[69], [70]. We then solve these differential equations numerically using the shooting method to determine the stretches. Once the stretches are determined, the charge on either electrode  $Q$  is the integral of the electric displacement over the area of the membrane  $Q = \int D\lambda_1\lambda_2 dA$ . Subsequently, the capacity of the balloon is  $C = Q/\phi$ .

## II.11. Experimental Results

A sample of elastomer material with diameter of 3 cm, thickness 210  $\mu\text{m}$  and mass 0.15 g (OP) or thickness 300  $\mu\text{m}$  and mass 0.21g (ZRU) is coated with carbon grease and mounted onto a pressure chamber. The pressure inside the chamber is measured with a pressure sensor (JUMO dTrans p30 40.4366) and the volume of the balloon is recorded with a high-speed camera at 250fps (JVC GC-PX10).

The electrical circuit shown in Figure II.12b consists of two large high voltage capacitors providing charge to the soft generator ( $C_{in}$ ) or receiving charge from the soft generator ( $C_{out}$ ). The capacitors have a capacity of 440nF@10kV each consisting of four 100nF and one 40nF capacitors from FTCap<sup>TM</sup> in parallel connection. The direction of charge transfer is passively controlled by two high voltage diodes (X100UFG from Voltage Multipliers Inc.) avoiding the need for actively switching relays. The whole circuit is isolated from external power supplies allowing for accurate measurement of the change of stored electrical energy by measuring the voltage change at the reservoirs  $\Delta\phi_{\{in,out\}}$  with an electrostatic voltmeter (TREK 341A). The net charge delivered to the soft generator is

$$\Delta Q_{net} = C_{in}\Delta\phi_{in} - C_{out}\Delta\phi_{out} \quad (\text{II.14})$$

The data of the pressure sensor and the electrostatic voltmeter is recorded by a LabView™ program and subsequently synchronized with the volume evolution measured by the high speed camera.

In Figure II.13b we show the evolution of the generators mechanical and electrical work-conjugate variables ( $p - V$  and  $\phi - Q_{net}$  respectively) during the 6<sup>th</sup> cycle of a multicycle experiment. The inflation process starts at  $t = 0s$  (point 4) and before that the voltage drops at the disconnected and charged membrane due to charge leakage. The voltage drops sharply due to the changing capacity and as it equals the voltage of the input reservoir at  $t = 0.34s$  charges are transferred to the generator until the volume reaches its maximum. At  $t = 1.73s$  the generator is deflated as quickly as possible, boosting the voltage up until it matches that of the output reservoir at  $t = 1.84s$  at which point the generator is discharged concluding the cycle at  $t = 1.85s$ . Afterwards the voltage of the generator again drops below that of the output reservoir due to the leaking of charge. At each instant the state of the soft generator is completely defined by each pair of work-conjugate variables  $p - V$  and  $\phi - Q_{net}$ . Figure II.13c follows the evolution of the state in the electrical work-conjugate plane resembling the schematics of Figure II.12a. The cycle is not closed as a total of  $5.5 \mu C$  of the input charge  $\Delta Q_{in} = 21.2 \mu C$  is leaked through the membrane and the net charge transferred to the generator after one full inflation-deflation cycle  $Q_{net} > 0$ . The specific electrical energy generated is obtained by integrating along the path in Figure II.13c which results to  $369 \text{ mJ/g}$  and a specific power of  $200 \text{ mW/g}$ . These are among the highest experimentally validated

values reported in literature for soft generators. The mechanical energy consumed during the conversion cycle is determined by the hysteresis area in Figure II.13d amounting to 5.1 J/g and thus the mechanical to electrical conversion efficiency is 7.2%. The hysteresis area is a result of mechanical losses (viscoelasticity, Mullins effect) and from conversion of mechanical energy. Without losses the area in the electrical and mechanical work conjugate plane will become equal and the efficiency would be 100%.

The typical conversion cycle depicted before (Figure II.12) is also used to assess the aptitude of ZRU for soft generators and results are shown in Figure II.14. The specific electrical energy generated in this experimental cycle was 217 mJ/g consuming mechanical work of 2.1J/g resulting in an mechanical to electrical conversion efficiency of 10.3%. As some charge leaked through the membrane (6.8 $\mu$ C) the cycle is not closed since more charge was transferred from the input reservoir to the membrane than transferred back to the output reservoir.

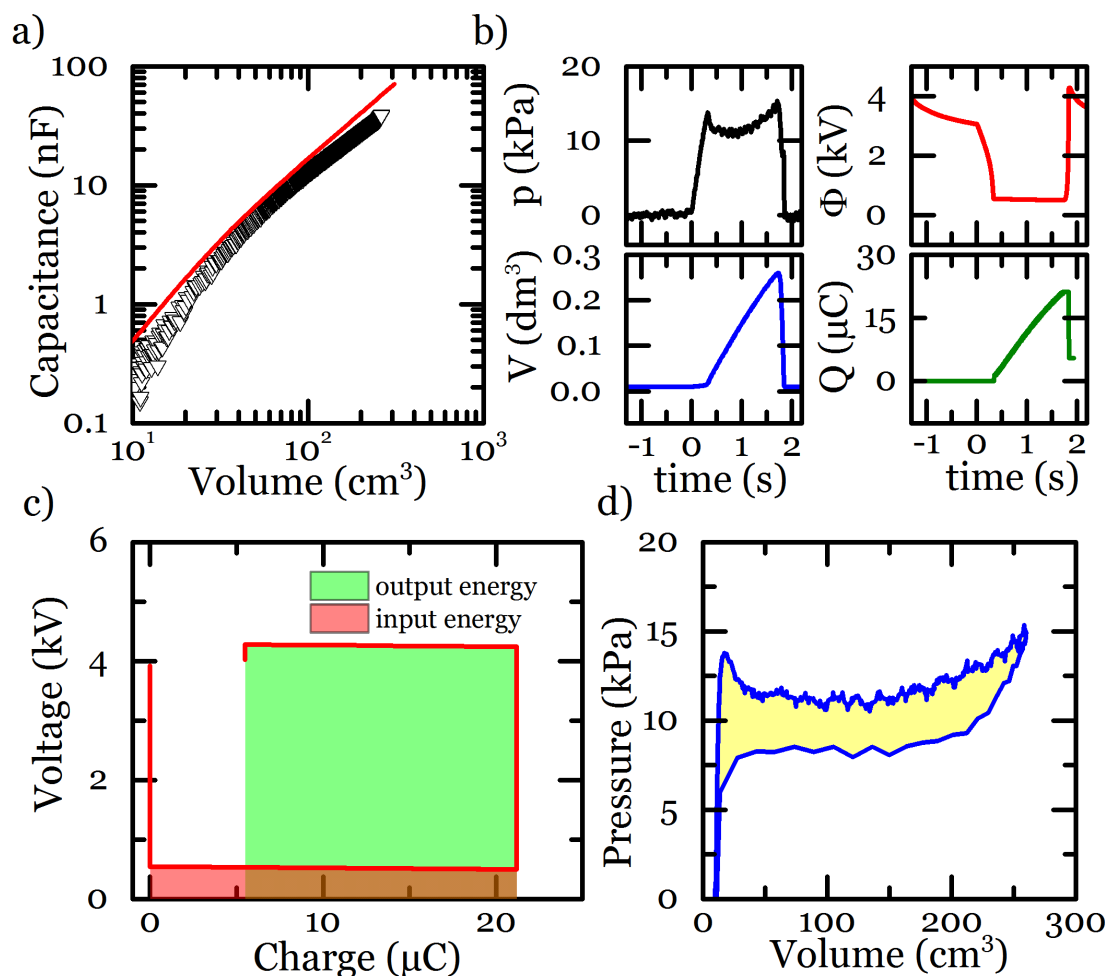


**Figure II.13. Experimental demonstration of high specific energy and power for a natural rubber based soft generator.** a) The electrical capacitance of the elastomer membrane changes by two orders of magnitude due to inflation. Experimental (black squares) and theoretical (red line) data for the capacitance show good agreement. b) Time course of mechanical and electrical work-conjugate variables (pressure  $p$  - volume  $V$  and voltage  $\phi$  - net charge  $Q$ ) during the 6<sup>th</sup> cycle of a measurement. c) Measured generator cycle depicted in the electrical work conjugate plane. The cycle is not closed due to charge leakage. The shaded areas visualize electrical input (red) and output (green) energy. The specific electrical energy generated in this cycle amounts to 369 mJ/g at an average power of 200 mW/g. d) Measured generator cycle depicted in the mechanical work conjugate plane. The enclosed area represents the supplied mechanical energy (5.1 J/g) yielding a mechanical to electrical energy conversion efficiency of 7.2%.

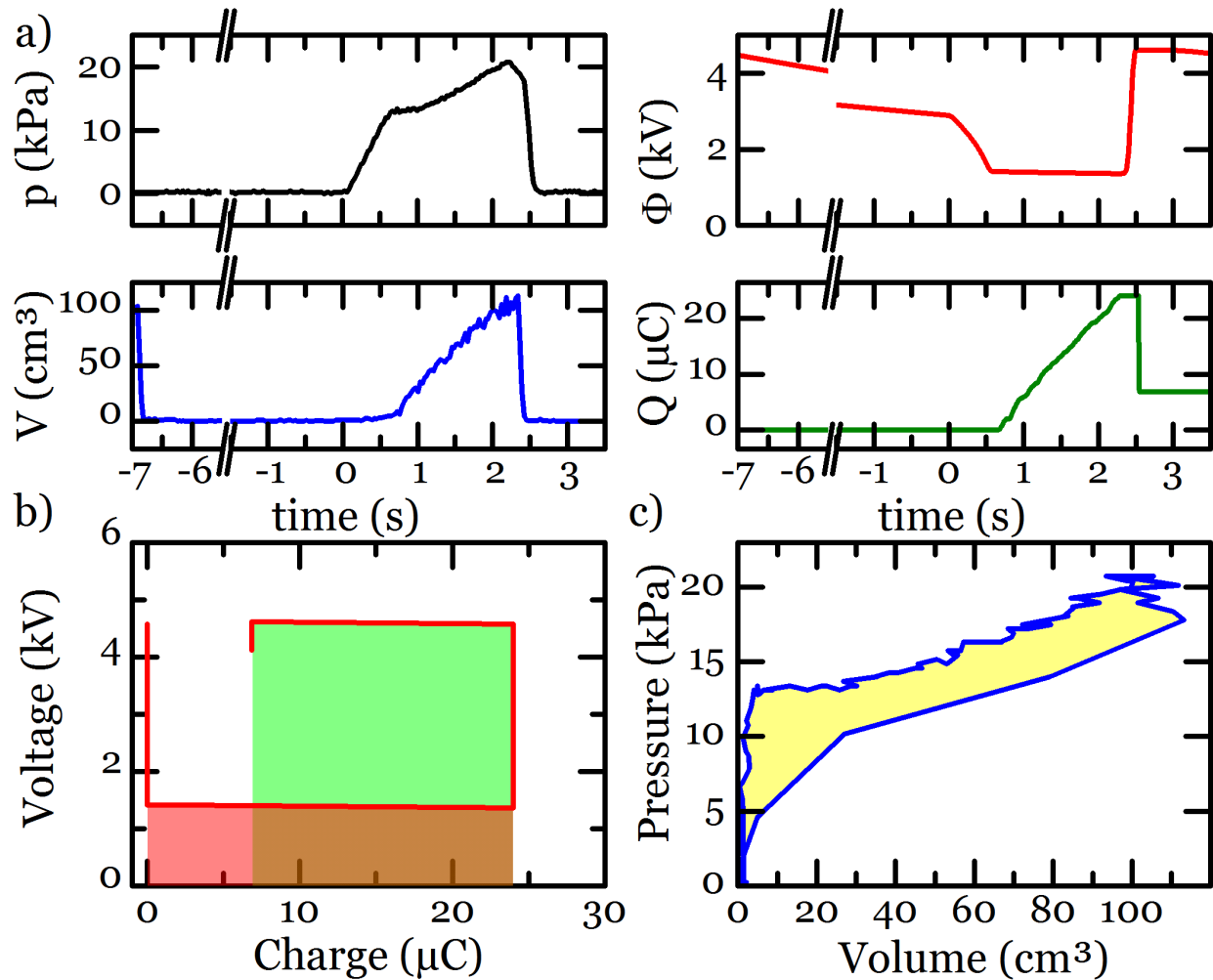


Figure II.14. Experimental harvesting cycle. a) The evolution of work conjugate variables ( $p - V$ ,  $\phi - Q$ ) in time. b) The path of the soft generators state through the electrical work-conjugate plane. The red shaded area shows electrical energy input (158mJ/g), and the green shaded area shows the output (375mJ/g) which totals in a net generated energy of 217 mJ/g. c) The path depicted in the mechanical work-conjugate plane.

## II.12. Conclusion

The material cost is essential to the feasibility of WECs using soft generators. Soft generators may not only be used in soft WECs but also in harvesting energy from waste heat [10], human gait[11], [72] and river flow [27] and other mechanical resources. We expect that material cost is generally significant for all small and large scale applications. In this work we show that NR is a very promising material as of its low cost (300 \$/t) and high energy conversion capability (3.5 J/g per cycle). Validation of an exemplary harvesting cycle yields a specific electrical energy generation of 369 mJ/g per cycle and 200 mW/g at an mechanical to electrical conversion efficiency of 11.6%. The high performance of OP is based on the high shear modulus  $\mu = 466$  kPa and high dielectric strength  $E_B(\lambda) = \lambda^{0.99} \times 96.5$  MV/m of NR compared to VHB4910™ ( $\mu = 52$  kPa,  $E_B = \lambda^{0.54} \times 68.6$  MV/m). This is not specific to OP but can be generalized to other natural rubbers as well as is shown by our analysis of ZRU. Using the experimental performance of NR we estimate the LCOE of soft WECs to be in the range 5.4 – 13.5 \$ct/kWh, thereby competing with existing technologies. Soft WECs provide high voltage direct current without the need for transformation and the wave energy resource is available at many coasts which are highly populated regions. Future materials designed specifically for high lifetime and high performance will improve the performance of soft WECs and as the technology is maturing the maintenance cost will decrease. The

success of PELAMIS™ indicates that public and political support is already enabling the construction of wave farms and with further support the harvesting of wave energy will find its place in the global energy mix providing clean and sustainable, low-cost electrical energy.

## II.13. References

- [1] J. Plante and S. Dubowsky, “On the performance mechanisms of Dielectric Elastomer Actuators,” *Sensors and Actuators A: Physical*, vol. 137, no. 1, pp. 96–109, Jun. 2007.
- [2] C. Keplinger, M. Kaltenbrunner, N. Arnold, and S. Bauer, “Rontgen’s electrode-free elastomer actuators without electromechanical pull-in instability,” *Proceedings of the National Academy of Sciences of the United States of America*, vol. 107, no. 10, pp. 4505–10, Mar. 2010.
- [3] S. Rosset, P. Dubois, M. Niklaus, and H. Shea, “Large Stroke miniaturized dielectric Elastomer Actuators,” in *IEEE Transducers*, 2009, pp. 2401–2404.
- [4] R. D. Kornbluh, R. Pelrine, H. Prahlaad, A. Wong-Foy, B. McCoy, S. Kim, J. Eckerle, and T. Low, “From boots to buoys: promises and challenges of dielectric elastomer energy harvesting,” in *Proceedings of SPIE*, 2011, vol. 7976, no. 1, p. 797605.
- [5] C. Jean-Mistral, S. Basrour, and J.-J. Chaillout, “Dielectric polymer: scavenging energy from human motion,” *Proceedings of SPIE*, vol. 6927, pp. 692716–692716–10, 2008.
- [6] H. Prahlaad, R. D. Kornbluh, R. Pelrine, S. Stanford, J. Eckerle, and S. Oh, “Polymer Power : Dielectric Elastomers and Their Applications in Distributed Actuation and Power Generation,” in *Proceedings of ISSS 2005*, 2005, no. 650, pp. 100–107.
- [7] S. Chiba, M. Waki, R. D. Kornbluh, and R. Pelrine, “Extending applications of dielectric elastomer artificial muscle,” *Proceedings of SPIE*, vol. 6524, pp. 652424–652424–5, 2007.

- [8] R. Pelrine, “High-Speed Electrically Actuated Elastomers with Strain Greater Than 100%,” *Science*, vol. 287, no. 5454, pp. 836–839, Feb. 2000.
- [9] P. Jean, A. Watzet, G. Ardoise, C. Melis, R. Van Kessel, A. Fourmon, E. Barrabino, J. Heemskerk, and J. P. Queau, “Standing wave tube electro active polymer wave energy converter,” in *Proceedings of SPIE*, 2012, p. 83400C–83400C–21.
- [10] P. Rothmund, “unpublished.”
- [11] R. Pelrine, R. D. Kornbluh, J. Eckerle, P. Jeuck, S. Oh, Q. Pei, and S. Stanford, “Dielectric elastomers: Generator mode fundamentals and applications,” in *Proceedings of SPIE*, 2001, vol. 4329, p. 148.
- [12] P. Brochu and Q. Pei, “Advances in Dielectric Elastomers for Actuators and Artificial Muscles,” *Macromolecular Rapid Communications*, vol. 31, no. 1, pp. 10–36, Jan. 2010.
- [13] C. Jean-mistral, “Récupération d ’ énergie mécanique par polymères électroactifs pour microsystèmes autonomes communicants,” 2008.
- [14] R. Kaltseis, C. Keplinger, R. Baumgartner, M. Kaltenbrunner, T. Li, P. Mächler, R. Schwödauer, Z. Suo, and S. Bauer, “Method for measuring energy generation and efficiency of dielectric elastomer generators,” *Applied Physics Letters*, vol. 99, no. 16, p. 162904, Oct. 2011.
- [15] C. Graf and J. Maas, “Electromechanical Energy Conversion using Dielectric Elastomer Generators,” *Energy Conversion*, pp. 834–837, 2010.
- [16] S. Chiba, M. Waki, R. D. Kornbluh, and R. Pelrine, “Innovative power generators for energy harvesting using electroactive polymer artificial muscles,” in *Proceedings of SPIE*, 2008, vol. 6927, pp. 692715–692715–9.
- [17] S. J. A. Koh, C. Keplinger, T. Li, S. Bauer, and Z. Suo, “Dielectric Elastomer Generators: How Much Energy Can Be Converted?,” *IEEE/ASME Transactions on Mechatronics*, vol. 16, no. 1, pp. 33–41, Feb. 2011.
- [18] J. R. Chaplin, F. J. M. Farley, M. E. Prentice, R. C. T. Rainey, S. J. Rimmer, and A. T. Roach, “Development of the ANACONDA all-rubber WEC,” in *Proceedings of 7th EWTEC*, 2007.
- [19] J. Mullaly, *The Laying of the Cable, Or the Ocean Telegraph*. D. Appleton and Company, 1858.
- [20] K. Gunn and C. Stock-Williams, “Quantifying the global wave power resource,” *Renewable Energy*, vol. 44, pp. 296–304, Aug. 2012.

- [21] “Electric Energy Consumption,” *wikipedia*, 2013. [Online]. Available: [http://en.wikipedia.org/wiki/Electric\\_energy\\_consumption](http://en.wikipedia.org/wiki/Electric_energy_consumption).
- [22] A. Brito e Melo and J. Huckerby, Eds., “Ocean Energy Systems: Annual Report 2011,” OES/International Energy Agency, Lisbon, Portugal, 2011.
- [23] R. Bedard, “Economic and Social Benefits from Wave Energy Conversion Marine Technology,” *Marine Technology Society Journal*, vol. 41, no. 3, pp. 44–50, Sep. 2007.
- [24] M. Previsic, R. Bedard, H. George, and O. Siddiqui, “E2I EPRI Global - 006A - SF: System Level Design , Performance and Costs for San Francisco California Pelamis Offshore Wave Power Plant,” 2004.
- [25] R. Bedard, G. Hagerman, M. Previsic, O. Siddiqui, R. Thresher, and B. Ram, “E2I EPRI Global WP 009 - US Rev2: Offshore Wave Power Feasibility Demonstration Project,” 2005.
- [26] Y. Liu, L. Liu, Z. Zhang, Y. Jiao, S. Sun, and J. Leng, “Analysis and manufacture of an energy harvester based on a Mooney-Rivlin–type dielectric elastomer,” *EPL (Europhysics Letters)*, vol. 90, no. 3, p. 36004, May 2010.
- [27] J. Maas and C. Graf, “Dielectric elastomers for hydro power harvesting,” *Smart Materials and Structures*, vol. 21, no. 6, p. 064006, Jun. 2012.
- [28] M. Previsic, O. Siddiqui, and R. Bedard, “E2I EPRI WP - US --002 Rev 4: Economic Assessment Methodology for Offshore Wave Power Plants,” 2004.
- [29] J. Hardisty, *The Analysis of Tidal Stream Power*. Chichester, UK: John Wiley & Sons, Ltd, 2009.
- [30] R. Paasch, K. Ruehl, J. Hovland, and S. Meicke, “Wave energy: a Pacific perspective.,” *Philosophical transactions. Series A, Mathematical, physical, and engineering sciences*, vol. 370, no. 1959, pp. 481–501, Jan. 2012.
- [31] B. Drew, a R. Plummer, and M. N. Sahinkaya, “A review of wave energy converter technology,” *Proceedings of the Institution of Mechanical Engineers, Part A: Journal of Power and Energy*, vol. 223, no. 8, pp. 887–902, Dec. 2009.
- [32] F. J. M. Farley, R. C. T. Rainey, and J. R. Chaplin, “Rubber tubes in the sea,” *Philosophical transactions. Series A, Mathematical, physical, and engineering sciences*, vol. 370, no. 1959, pp. 381–402, Jan. 2012.
- [33] J. Hayward and P. Osman, “The potential of wave energy,” 2011.
- [34] U. Eia, *Annual Energy Outlook 2011*, vol. 0383, no. April. Energy Information Administration, 2011, p. 236.

- [35] C. McGowin, R. Bedard, S. Cardoso, D. O'Connor, T. Peterson, N. Lenssen, and N. Enbar, "Renewable Energy Technical Assessment Guide —TAG-RE: 2006. EPRI," Palo Alto, CA, 2007.
- [36] P. Osman, S. Behrens, D. Griffin, J. Hayward, M. Hemer, C. Knight, S. McGarry, and J. Wright, "Ocean renewable energy: 2015-2050," 2012.
- [37] D. Weisser, "A guide to life-cycle greenhouse gas (GHG) emissions from electric supply technologies," *Energy*, vol. 32, no. 9, pp. 1543–1559, Sep. 2007.
- [38] R. Kenny, C. Law, and J. M. Pearce, "Towards real energy economics: Energy policy driven by life-cycle carbon emission," *Energy Policy*, vol. 38, no. 4, pp. 1969–1978, Apr. 2010.
- [39] M. Lenzen, "Life cycle energy and greenhouse gas emissions of nuclear energy: A review," *Energy Conversion and Management*, vol. 49, no. 8, pp. 2178–2199, 2008.
- [40] K. a. Kelly, M. C. McManus, and G. P. Hammond, "An energy and carbon life cycle assessment of tidal power case study: The proposed Cardiff–Weston severn barrage scheme," *Energy*, vol. 44, no. 1, pp. 692–701, Aug. 2012.
- [41] R. Parker, G. Harrison, and J. Chick, "Energy and carbon audit of an offshore wave energy converter," *Journal of Power and Energy*, vol. 221, no. 8, pp. 1119–1130, 2007.
- [42] M. O'Connor, T. Lewis, and G. Dalton, "Techno-economic performance of the Pelamis P1 and Wavestar at different ratings and various locations in Europe," *Renewable Energy*, vol. 50, pp. 889–900, Feb. 2013.
- [43] S. Chu and A. Majumdar, "Opportunities and challenges for a sustainable energy future.," *Nature*, vol. 488, no. 7411, pp. 294–303, Aug. 2012.
- [44] W. Jawjit, C. Kroeze, and S. Rattanapan, "Greenhouse gas emissions from rubber industry in Thailand," *Journal of Cleaner Production*, vol. 18, no. 5, pp. 403–411, Mar. 2010.
- [45] B. Brandt, E. Kletzer, H. Pilz, D. Hadzhiyska, and P. Seizov, "Silicone-Chemistry Carbon Balance," 2012.
- [46] G. Hagerman and G. Scott, "Mapping and Assessment of the United States Ocean Wave Energy Resource 2011," 2011.
- [47] "Ocean Energy Systems: Annual Report 2007," 2007.
- [48] K. Ummel and D. Wheeler, "Desert Power : The Economics of Solar Thermal Electricity for Europe , North Africa , and the Middle East," 2008.

- [49] “Report of the IGA to the UN Commission on Sustainable Development, Session 9 (CSD-9): Contribution of Geothermal Energy to Sustainable Development,” New York, 2001.
- [50] A. Holm, L. Blodgett, D. Jennejohn, and K. Gawell, “Geothermal Energy: International Market Update May 2010,” 2010.
- [51] M. Z. Jacobson and C. L. Archer, “Saturation wind power potential and its implications for wind energy.,” *Proceedings of the National Academy of Sciences of the United States of America*, vol. 109, no. 39, pp. 15679–84, Sep. 2012.
- [52] “Worldwide electricity production from renewable resources,” 2012.
- [53] “Photovoltaic Barometer,” 2012.
- [54] “Renewable Energy Essentials: Hydropower,” 2010.
- [55] S. Solomon, D. Qin, M. Manning, Z. Chen, M. Marquis, K. B. Averyt, M. Tignor, and H. L. Miller, *IPCC, 2007: Climate Change 2007: The Physical Science Basis. Contribution of Working Group I to the Fourth Assessment Report of the Intergovernmental Panel on Climate Change*, vol. Geneva, no. November. Cambridge University Press, 2007, p. 996.
- [56] S. J. A. Koh, X. Zhao, and Z. Suo, “Maximal energy that can be converted by a dielectric elastomer generator,” *Applied Physics Letters*, vol. 94, no. 26, p. 262902, 2009.
- [57] A. N. Gent, “A New Constitutive Relation for Rubber,” *Rubber Chemistry and Technology*, vol. 69, no. 1, pp. 59–61, Mar. 1996.
- [58] Z. Suo, “Theory of dielectric elastomers,” *Acta Mechanica Solida Sinica*, vol. 23, no. 6, pp. 549–578, Apr. 2010.
- [59] M. Kolloosche, M. Melzer, A. Becker, H. Stoyanov, D. N. McCarthy, H. Ragusch, and G. Kofod, “The influence of mechanical properties in the electrical breakdown in polystyrene-ethylene-butadiene-styrene thermoplastic elastomer,” *Proceedings of SPIE*, vol. 7287, pp. 728729–728729–9, 2009.
- [60] C. Jean-Mistral, A. Sylvestre, S. Basrour, and J.-J. Chaillout, “Dielectric properties of polyacrylate thick films used in sensors and actuators,” *Smart Materials and Structures*, vol. 19, no. 7, p. 075019, Jul. 2010.
- [61] J. Huang, S. Shian, Z. Suo, and david r Clarke, “Maximizing the energy density of dielectric elastomer generators using equi-biaxial loading,” *Advanced Functional Materials*, vol. unpub, 2013.
- [62] A. Tröls, A. Kogler, R. Baumgartner, R. Kaltseis, C. Keplinger, R. Schwödiauer, I. M. Graz, and S. Bauer, “Stretch dependence of the electrical breakdown strength and

- dielectric constant of dielectric elastomers,” *Smart Materials and Structures*, vol. unpub, 2013.
- [63] R. S. Rivlin and a. G. Thomas, “Rupture of rubber. I. Characteristic energy for tearing,” *Journal of Polymer Science*, vol. 10, no. 3, pp. 291–318, Mar. 1953.
- [64] M. Pharr, J.-Y. Sun, and Z. Suo, “Rupture of a highly stretchable acrylic dielectric elastomer,” *Journal of Applied Physics*, vol. 111, no. 10, p. 104114, 2012.
- [65] A. Griffith, “The phenomena of rupture and flow in solids,” *Philosophical transactions of the royal society of ...*, vol. 221, pp. 163–198, 1921.
- [66] a. Dorfmann and R. W. Ogden, “A constitutive model for the Mullins effect with permanent set in particle-reinforced rubber,” *International Journal of Solids and Structures*, vol. 41, no. 7, pp. 1855–1878, Apr. 2004.
- [67] F. Bueche, “Molecular basis for the mullins effect,” *Journal of Applied Polymer Science*, vol. 4, no. 10, pp. 107–114, Jul. 1960.
- [68] C. Keplinger, T. Li, R. Baumgartner, Z. Suo, and S. Bauer, “Harnessing snap-through instability in soft dielectrics to achieve giant voltage-triggered deformation,” *Soft Matter*, 2012.
- [69] J. Zhu, S. Cai, and Z. Suo, “Resonant behavior of a membrane of a dielectric elastomer,” *International Journal of Solids and Structures*, vol. 47, no. 24, pp. 3254–3262, Dec. 2010.
- [70] T. Li, C. Keplinger, R. Baumgartner, S. Bauer, W. Yang, and Z. Suo, “Giant voltage-induced deformation in dielectric elastomers near the verge of snap-through instability,” *Journal of the Mechanics and Physics of Solids*, vol. 61, no. 2, pp. 611–628, Feb. 2013.
- [71] X. Zhao, W. Hong, and Z. Suo, “Electromechanical hysteresis and coexistent states in dielectric elastomers,” *Physical Review B*, vol. 76, no. 13, p. 134113, Oct. 2007.
- [72] T. McKay, B. M. O’Brien, E. Calius, and I. Anderson, “Self-priming dielectric elastomer generators,” *Smart Materials and Structures*, vol. 19, no. 5, p. 055025, May 2010.
- [73] D. A. Bruzewicz, M. Reches, and G. M. Whitesides, “Low-cost printing of poly(dimethylsiloxane) barriers to define microchannels in paper,” *Analytical chemistry*, vol. 80, no. 9, pp. 3387–92, May 2008.